Article

TRANSPARENT PROCESS

THE EMBO JOURNAL

Bassoon-disruption slows vesicle replenishment and induces homeostatic plasticity at a CNS synapse

Alejandro Mendoza Schulz[1,2,3], Zhizi Jing[2,3,4], Juan María Sánchez Caro[1], Friederike Wetzel[2,5], Thomas Dresbach[2,5], Nicola Strenzke[2,4,***], Carolin Wichmann[2,6,**] & Tobias Moser[1,2,7,8,*]

Abstract

Endbulb of Held terminals of auditory nerve fibers (ANF) transmit auditory information at hundreds per second to bushy cells (BCs) in the anteroventral cochlear nucleus (AVCN). Here, we studied the structure and function of endbulb synapses in mice that lack the presynaptic scaffold bassoon and exhibit reduced ANF input into the AVCN. Endbulb terminals and active zones were normal in number and vesicle complement. Postsynaptic densities, quantal size and vesicular release probability were increased while vesicle replenishment and the standing pool of readily releasable vesicles were reduced. These opposing effects canceled each other out for the first evoked EPSC, which showed unaltered amplitude. We propose that ANF activity deprivation drives homeostatic plasticity in the AVCN involving synaptic upscaling and increased intrinsic BC excitability. *In vivo* recordings from individual mutant BCs demonstrated a slightly improved response at sound onset compared to ANF, likely reflecting the combined effects of ANF convergence and homeostatic plasticity. Further, we conclude that bassoon promotes vesicular replenishment and, consequently, a large standing pool of readily releasable synaptic vesicles at the endbulb synapse.

Keywords active zone; bassoon; endbulb of Held; homeostatic plasticity; vesicle replenishment

Subject Categories Membrane & Intracellular Transport; Neuroscience

DOI 10.1002/embj.201385887 | Received 5 June 2013 | Revised 5 November 2013 | Accepted 7 November 2013 | Published online 17 January 2014

EMBO Journal (2014) 33, 512–527

Introduction

Presynaptic terminals are complex structures enabling vesicles to cycle between functionally different pools and to undergo exo- and endocytosis in a tightly regulated manner (Neher & Sakaba, 2008; Alabi & Tsien, 2012; Südhof, 2012). The active zones (AZs) of exocytosis are membrane domains that feature a rich network of proteins and therefore appear as dense structures in electron microscopy. While the proteins mediating vesicle fusion at central synapses have been characterized quite well, less is known about the role of scaffold proteins (or cytomatrix of the active zone (CAZ) proteins) in synaptic transmission. Apart from co-determining the structure of the AZ, CAZ proteins are thought to modulate vesicle recruitment, docking, priming, Ca^{2+} channel organization, coupling of Ca^{2+} influx to release-ready vesicles and between exo- and endocytic sites (Gundelfinger & Fejtova, 2012; Haucke *et al*, 2011; Rutherford & Pangršič, 2012; Hallermann & Silver, 2013). Thereby, in a manner depending on the precise CAZ composition, they lend plasticity and specificity to synapses enabling synaptic diversity (Zhai & Bellen, 2004). CAZ proteins encompass at least six protein families: Munc13s, Rab-interacting molecules (RIMs), RIM-binding proteins, ELKS/CAST proteins, piccolo and bassoon, and the liprins-α (Gundelfinger & Fejtova, 2012). Unlike the others, bassoon is believed to be vertebrate-specific (tom Dieck *et al*, 1998; Altrock *et al*, 2003). Bassoon, a large 420 kDa multidomain protein (tom Dieck *et al*, 1998), interacts with presynaptic proteins including CAST (Ohtsuka *et al*, 2002; Takao-Rikitsu *et al*, 2004), RIM (Wang *et al*, 2009), Munc13-1 (Wang *et al*, 2009), Ribeye (tom Dieck *et al*, 2005) and Mover (Kremer *et al*, 2007). While bassoon is generally found in

1 InnerEarLab, Department of Otolaryngology, University Medical Center Göttingen, Göttingen, Germany
2 Collaborative Sensory Research Center 889, University Medical Center Göttingen, Göttingen, Germany
3 IMPRS Neuroscience, Göttingen Graduate School for Neuroscience and Molecular Biosciences, Göttingen, Germany
4 Auditory Systems Physiology Group, InnerEarLab, Department of Otolaryngology and Collaborative Sensory Research Center 889, University Medical Center Göttingen, Göttingen, Germany
5 Department of Anatomy and Embryology, Center of Anatomy, University Medical Center Göttingen, Göttingen, Germany
6 Molecular Architecture of Synapses Group, InnerEarLab, Department of Otolaryngology and Collaborative Sensory Research Center 889, University Medical Center Göttingen, Göttingen, Germany
7 Center for Nanoscale Microscopy and Molecular Physiology of the Brain, University of Göttingen, Göttingen, Germany
8 Bernstein Center for Computational Neuroscience, University of Göttingen, Göttingen, Germany
*Corresponding author. Tel: +49 551 3922803; Fax: +49 551 3912950; E-mail: tmoser@gwdg.de
**Corresponding author. Tel: +49 551 3922604; Fax: +49 551 3912950; E-mail: cwichma@gwdg.de
***Corresponding author. Tel: +49 551 399688; Fax: +49 551 3912950; E-mail: nstrenzke@med.uni-goettingen.de

central synapses of vertebrates, neuromuscular junction (Carlson *et al*, 2010; Chen *et al*, 2011) as well as in sensory ribbon synapses (Dick *et al*, 2001; Khimich *et al*, 2005) it seems to assume different roles at these synapses. Disruption of bassoon function by deletion of exons 4 and 5 of the *Bsn* gene that code for a large central part of bassoon in mice ($Bsn^{\Delta Ex4/5}$) led to a higher number of presynaptically silent synapses in cultured hippocampal neurons (Altrock *et al*, 2003), while the remaining synaptic transmission of the functional synapses was unaltered (Altrock *et al*, 2003; Mukherjee *et al*, 2010). Working on a cerebellar synapse with high transmission rate an impairment of vesicle replenishment was found in $Bsn^{\Delta Ex4/5}$ and a bassoon gene trap mouse mutant (Hallermann *et al*, 2010). However, potential accompanying ultrastructural and molecular changes remain to be investigated. Robust morphological and functional phenotypes were observed at the ribbon synapses of retinal photoreceptors (Dick *et al*, 2003) and cochlear inner hair cells (Khimich *et al*, 2005; Buran *et al*, 2010; Frank *et al*, 2010; Jing *et al*, 2013) of $Bsn^{\Delta Ex4/5}$ mice including detached or missing ribbons and a reduced rate of transmitter release. In hair cells, fewer membrane-tethered vesicles and Ca^{2+} channels lead to a reduced number of readily releasable vesicles and their replenishment is impaired in addition (Frank *et al*, 2010). Consistent with the reduction of exocytosis from inner hair cells, the postsynaptic auditory nerve fibers (ANFs) exhibited approximately halved sound-evoked spiking rates (Buran *et al*, 2010; Jing *et al*, 2013) and the compound action potential of the spiral ganglion was much reduced (Khimich *et al*, 2005; Buran *et al*, 2010; Jing *et al*, 2013). However, the subsequent auditory brainstem responses were better maintained, suggesting some compensatory mechanism in the AVCN. Whether such improved synchronicity of auditory signaling results from the convergent ANF input to BCs or the AVCN undergoes homeostatic plasticity in response to the reduced ANF spike rates remained to be investigated.

Here, we studied synaptic transmission at the endbulb of Held of bassoon mouse mutants, the first central synapse of the auditory system (Von Gersdorff & Borst, 2002; O'Neil *et al*, 2011; Wang *et al*, 2011), where large calyceal presynaptic terminals of auditory nerve fibers use hundreds of small AZs to provide strong and convergent excitatory input to BCs (Nicol & Walmsley, 2002). Together, these AZs account for a large readily releasable pool of vesicles, which enables high release rates that together with fast AMPA receptors and efficient glutamate clearance contribute to reliable and temporally precise transmission at hundreds of spikes per second (Wang *et al*, 2011). We combined quantitative light and electron microscopy, *in vitro* electrophysiology in acute brainstem slices and *in vivo* extracellular recordings of sound-driven activity to study the role of bassoon in synaptic transmission from ANFs to BCs and potential homeostatic plasticity in hearing impaired $Bsn^{\Delta Ex4/5}$ mice.

Results

Molecular composition and number of AZs in the endbulb of Held

We used immunohistochemistry in order to elucidate effects of bassoon disruption and potential homeostatic plasticity on the convergence of ANFs, the number of AZs and their molecular composition. After the onset of hearing (p15 to p23), BCs of the mouse AVCN receive glutamatergic input of 2–3 (spherical BCs) and 3–5 (globular BCs) auditory nerve fibers (Cao & Oertel, 2010) via large endbulb synapses. The number of endbulbs converging onto individual BCs was quantified by reconstructing calretinin-stained endbulbs (Lohmann & Friauf, 1996; Caicedo *et al*, 1997; Chanda & Xu-Friedman, 2010a) as exemplified in Fig 1A and explained in the Materials and Methods section. We did not attempt to discriminate spherical BCs and globular BCs assuming that bassoon disruption affects their endbulb synapses to a similar extent. However, we likely favored analysis of spherical BCs, as is indicated by the average number of endbulbs per BC (Fig 1B, 3.0 ± 0.21 for Bsn^{wt} ($n = 12$)). The number of endbulbs per BC was unchanged in $Bsn^{\Delta Ex4/5}$ mice (3.1 ± 0.17, $n = 16$ BCs), indicating unaltered convergence (Fig 1B). We did not distinguish endbulb and excitatory bouton-like synapses, given that endbulbs contribute the vast majority of excitatory AZs (Nicol & Walmsley, 2002; Gómez-Nieto & Rubio, 2009). In addition to the excitatory input, BCs also receive inhibitory input (Wu & Oertel, 1984; Babalian *et al*, 2002; Kopp-Scheinpflug *et al*, 2002; Gómez-Nieto & Rubio, 2009). We discriminated such inhibitory synapses from excitatory ones by co-immunolabeling them for the vesicular GABA transporter (VGAT, Fig 1A) or for gephyrin, a postsynaptic scaffold of inhibitory synapses (Fig 2).

In order to study the molecular composition of the presynaptic AZ in endbulbs we analyzed the expression and localization of the CAZ proteins bassoon, piccolo, Munc13-1 and RIM2, in Bsn^{wt} and $Bsn^{\Delta Ex4/5}$ mice. Moreover, in a small set of experiments we also observed spots of CAST and ELKS immunofluorescence around Bsn^{wt} BCs (data not shown). All CAZ proteins assumed a spot-like immunofluorescence pattern surrounding the BCs, which most likely reflected AZs (Figs 1 and 2). We immunolabeled for bassoon and piccolo to investigate the expression and localization relative to the AZ of full-length bassoon (Fig 1C, Bsn-sap7f antibody (tom Dieck *et al*, 1998)) and a truncated bassoon fragment that remains expressed in $Bsn^{\Delta Ex4/5}$ mice (Altrock *et al*, 2003) and is only recognized by an antibody directed towards the C-terminus (Fig 1C). In Bsn^{wt} AVCN, all three labels overlapped (Fig 1D and F), indicating that bassoon and piccolo coexist at the majority of the AZs facing a BC. In addition, there were some AZs that selectively contained bassoon or piccolo, observations that are generally consistent with findings at the calyx of Held (Dondzillo *et al*, 2010). However, while at the calyx of Held approximately 60% of bassoon and piccolo spots were found to overlap, we observed a larger fraction of piccolo AZs containing also bassoon (Bsn-sap7f: 66%; Bsn-c-term.: 84%, with a criterion for the center of immunofluorescence mass distance of 500 nm in xy and 1,500 nm in z, see Materials and Methods). As expected, AZs of $Bsn^{\Delta Ex4/5}$ BCs lacked Bsn-sap7f-immunofluorescence (Fig 1E,F) and only unspecific ribbon-like fluorescence outside the BC, likely reflecting capillaries and present also in Bsn^{wt}, remained. Consistent with previous observations at other synapses (Dresbach *et al*, 2003; Frank *et al*, 2010) the remaining fragment was not or less efficiently integrated in to the AZ, as is evident from the diffuse and weak labeling for the truncated bassoon fragment that less accurately co-localized with piccolo. The center of mass distance of the nearest neighboring spots of piccolo and bassoon (Bsn-c-term. antibody) was significantly larger and more variable (F–test: $P < 0.001$) in $Bsn^{\Delta Ex4/5}$ terminals than in Bsn^{wt} (Fig 1G). Therefore, we assume that AZs $Bsn^{\Delta Ex4/5}$ endbulbs lack functional bassoon.

The experiments described above did not discriminate excitatory and inhibitory AZs. In order to approximate the number of

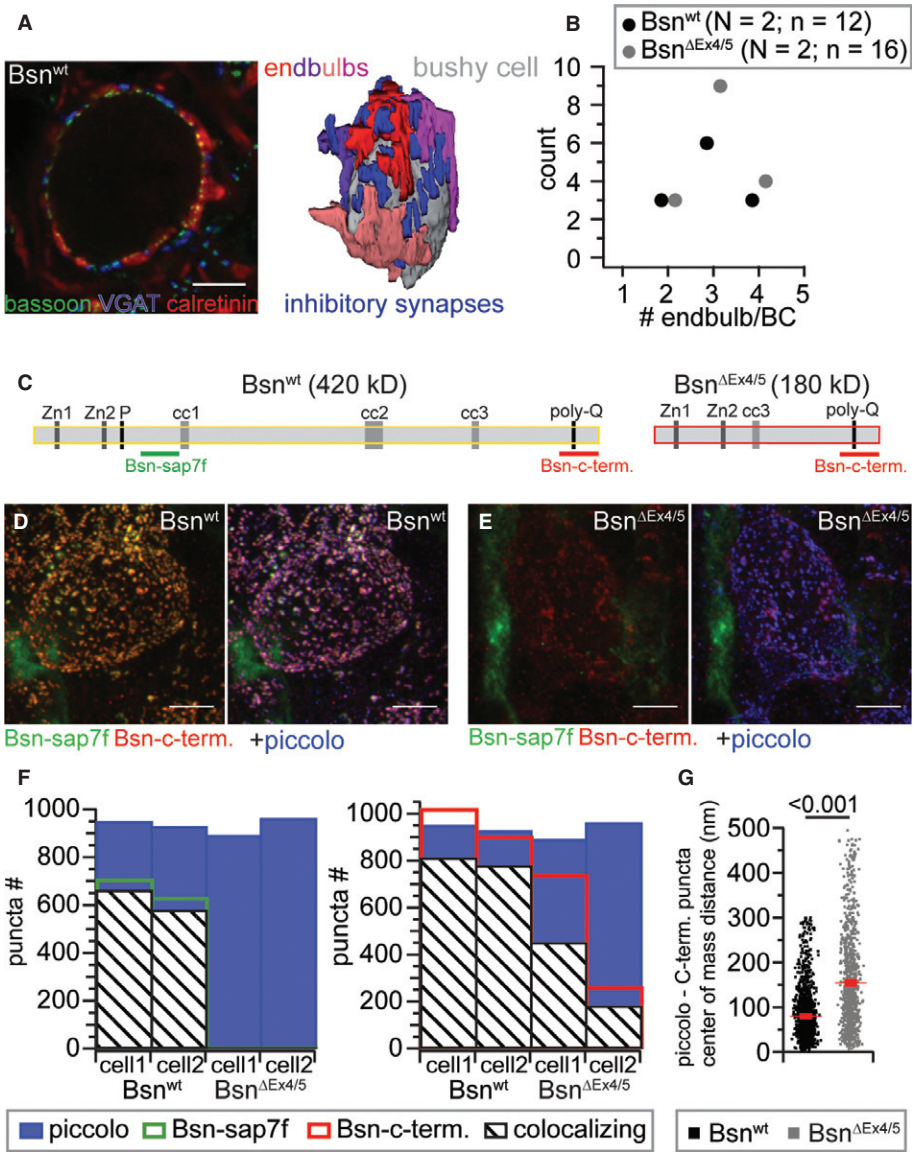

Figure 1. Number of converging endbulbs and bassoon immunolocalization in the AVCN of Bsn^{wt} and Bsn$^{\Delta Ex4/5}$ mice.

A Single confocal section from a stack (left) used for reconstruction of endbulb terminals (right, four endbulbs converging onto the BC in this example), immunolabeled for calretinin (red) as an endbulb marker, bassoon (green) as a marker for AZs and VGAT (blue) as a marker for inhibitory synapses.

B The number of endbulb terminals converging onto a BC remained unchanged in Bsn$^{\Delta Ex4/5}$ mice (*N*, number of animals; *n*, number of BCs).

C Domain structure of bassoon and the Bsn$^{\Delta Ex4/5}$ fragment including the epitopes utilized for immunolabeling.

D, E Projection of a confocal image stack labeled for the two bassoon epitopes and piccolo of a Bsn^{wt} (D) and a Bsn$^{\Delta Ex4/5}$ (E) BC.

F Number of puncta and fraction of colocalizing bassoon puncta (left, Bsn-sap7f AB; right Bsn-c-term. AB) with piccolo of two BC for each genotype.

G Center of mass distance between all colocalizing Bsn-c-term. and piccolo puncta of the four cells depicted in (F), illustrating that the Bsn$^{\Delta Ex4/5}$ fragment is not as tightly confined to AZs as wild-type bassoon.

excitatory AZs onto Bsn^{wt} and Bsn$^{\Delta Ex4/5}$ BCs, mostly reflecting AZs of endbulbs, we counted the piccolo-positive puncta without and with juxtaposition to inhibitory postsynapses marked by gephyrin immunofluorescence in stacks of confocal sections. Subtracting the number of gephyrin-associated piccolo puncta yielded the number of excitatory AZs, which was unchanged in Bsn$^{\Delta Ex4/5}$ mutants (Fig 2B). When divided by the average number of endbulb terminals, the average number of AZs per endbulb was 126 and 121 for Bsn^{wt} (n = 12) and Bsn$^{\Delta Ex4/5}$ (n = 12), respectively. These AZ numbers are comparable to the on average 155 AZs found in four reconstructed endbulbs in a previous serial section electron microscopy study (Nicol & Walmsley, 2002). The cumulative pixel-intensities of piccolo-immunofluorescence spots around BCs in AVCN sections of Bsn^{wt} and Bsn$^{\Delta Ex4/5}$ mice, which we processed in parallel, revealed significantly more immunofluorescence for Bsn$^{\Delta Ex4/5}$ AZs. This indicated a likely compensatory upregulation of piccolo protein at

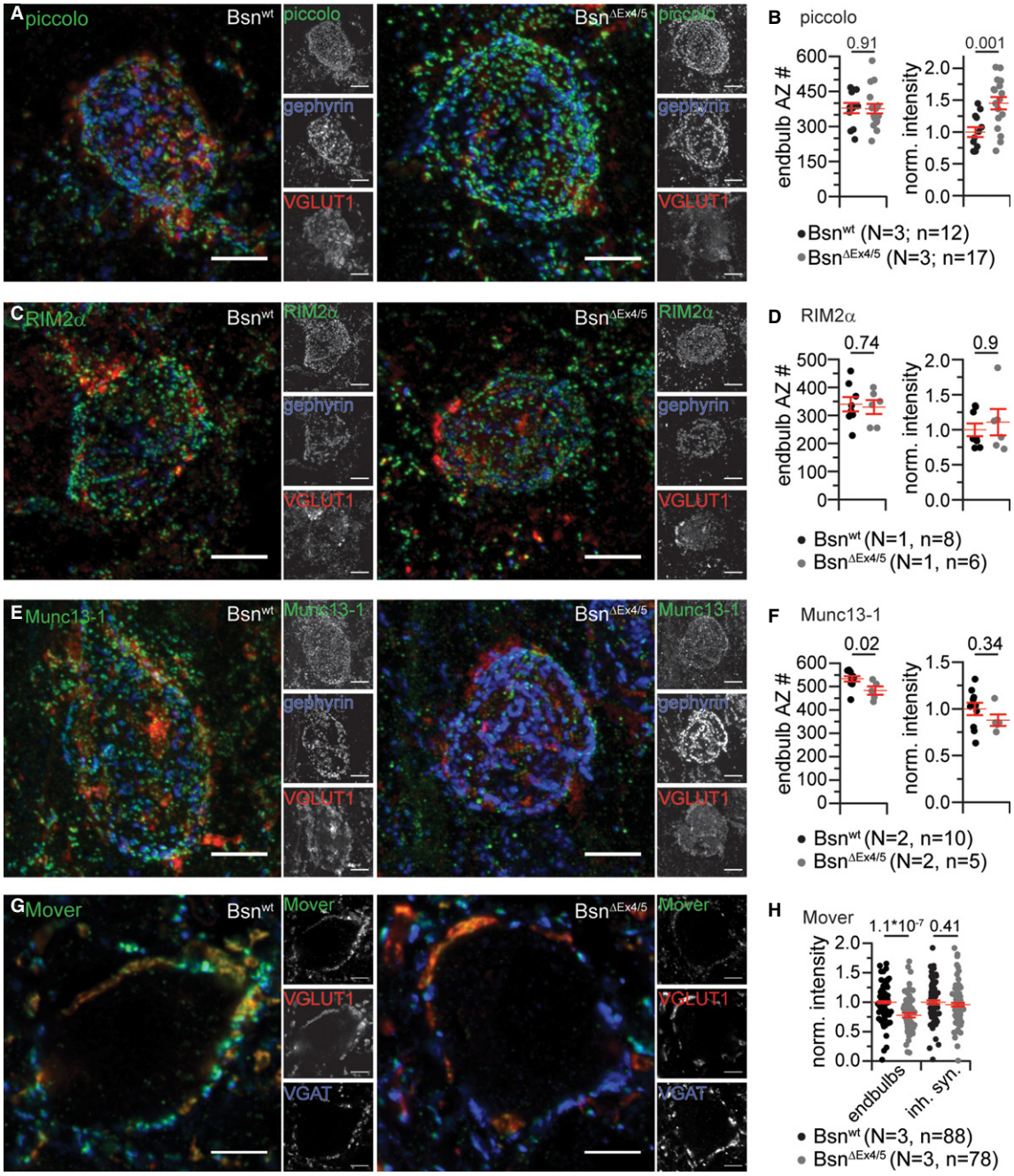

Figure 2. Molecular composition of murine endbulb of Held synapses..

A Projections of confocal image stacks of Bsn^{wt} (left) and $Bsn^{\Delta Ex4/5}$ (right) AVCN labeled for piccolo (green), gephyrin (blue) and VGLUT1 (red).

B The number of endbulb AZs was estimated from the number of piccolo puncta surrounding a bushy cell, excluding the ones colocalizing with gephyrin (*N*, number of animals; *n*, number of BCs). While the number of piccolo puncta was found to be unchanged in mutant endbulbs, the fluorescence intensity of piccolo puncta was significantly increased.

C, D Projections of a confocal image stacks labeled for RIM2α (green) co-labeled for gephyrin (blue) and VGLUT1 (red) (C), and quantification of RIM2α-positive endbulb AZ number and fluorescence intensity (D).

E, F Projections of a confocal image stacks labeled for Munc13-1 (green) co-labeled for gephyrin (blue) and VGLUT1 (red) (E), and quantification of Munc13-1-positive endbulb AZ number and fluorescence intensity (F).

G Single confocal sections labeled for Mover (green), gephyrin (blue) and VGLUT1 (red) showing a significant reduction of Mover fluorescence intensity in $Bsn^{\Delta Ex4/5}$ endbulbs but unchanged intensity in inhibitory terminals.

Data information: All scale bars, 5 μm.

endbulb AZs upon the loss of full-length bassoon (Fig 2B). In addition, we studied RIM2α and Munc13-1, which served as exemplary CAZ constituents. The number and fluorescence intensity of RIM2α- and Munc13-1-immunoreactive spots was largely unaltered in $Bsn^{\Delta Ex4/5}$ endbulbs (Fig 2C–F). In search for molecular changes resulting from bassoon disruption we also analyzed the immunofluorescence intensity of the recently identified bassoon-interacting, vesicle-associated protein Mover (Kremer *et al*, 2007) that appears to regulate release probability at the calyx of Held (Körber, 2011). Mover was present in excitatory (VGLUT1-positive) and in inhibitory (VGAT-positive) terminals. The Mover immunofluorescence was significantly reduced in VGLUT1-positive (approximately 22 %) but not in VGAT-positive terminals. The VGLUT1 immunofluorescence was unaltered (Supplementary Fig S1). We conclude that, despite the lack of functional bassoon, endbulbs and excitatory AZs were formed in normal quantity. While the abundance of RIM2α and Munc13-1 was unchanged, piccolo was up-regulated whereas the putative bassoon-effector Mover was down-regulated in endbulbs.

Larger postsynaptic densities and increased quantal size

Using electron microscopy we probed for potential effects of bassoon disruption on synaptic ultrastructure of excitatory (asymmetric) synapses onto BCs in ultrathin (55 nm) random AVCN sections (Fig 3). We measured the length of the postsynaptic density (PSD) and found larger PSDs in BCs (Fig 3C; Bsn^{wt}: $n = 47$, $Bsn^{\Delta Ex4/5}$ $n = 54$). We then compared the vesicle distribution by counting synaptic vesicles in five 40 nm bins from the presynaptic membrane into the cytosol of the presynaptic terminal (Supplementary Fig S2). We observed a trend towards fewer membrane-proximal vesicles in $Bsn^{\Delta Ex4/5}$ excitatory synapses (first bin), which became significant when related to the PSD length (Fig 3D). The number of vesicles in direct contact with the presynaptic plasma membrane (Fig 3D) was unaltered, as were the vesicle counts for the other bins and the vesicle size (Supplementary Fig S2). Given that bassoon is part of the CAZ we also counted presynaptic dense projections (DP), electron-dense appearing specializations that extend from the cytomatrix into the cytoplasm and tether synaptic vesicles (Zhai & Bellen, 2004) and found their number unaltered in $Bsn^{\Delta Ex4/5}$ excitatory synapses (Supplementary Fig S2).

Since the increased PSD length may reflect a larger cluster of AMPA receptors, we compared mEPSC amplitudes (quantal size) between BCs of both genotypes in acute slice preparations of the AVCN. Recordings were restricted to the anterior- and dorsal-most region of the AVCN as illustrated in Supplementary Fig S3. We found a significant increase in the amplitude of the mEPSCs (Fig 4B; Bsn^{wt}: $n = 38$, $Bsn^{\Delta Ex4/5}$: $n = 51$), while their frequency and kinetics were unchanged (Fig 4C–F). In conclusion, we found a larger quantal size at $Bsn^{\Delta Ex4/5}$ synapses, which we attribute to a larger number of AMPA receptors, likely reflecting homeostatic synaptic scaling. We also analyzed further parameters relevant to homeostatic plasticity and observed a reduced BC size. BC soma size was estimated from immunofluorescence analysis, in which we obtained volume estimates from fitting spheres to the halo of piccolo-positive AZs and found smaller volumes for $Bsn^{\Delta Ex4/5}$ BCs ($1077.5 \pm 53.0\ \mu m^3$ in $Bsn^{\Delta Ex4/5}$ vs. $1362.5 \pm 55.0\ \mu m^3$ in Bsn^{wt}, $P = 0.0006$, Bsn^{wt}: $n = 18$, $Bsn^{\Delta Ex4/5}$: $n = 21$). A smaller BC size was also indicated by

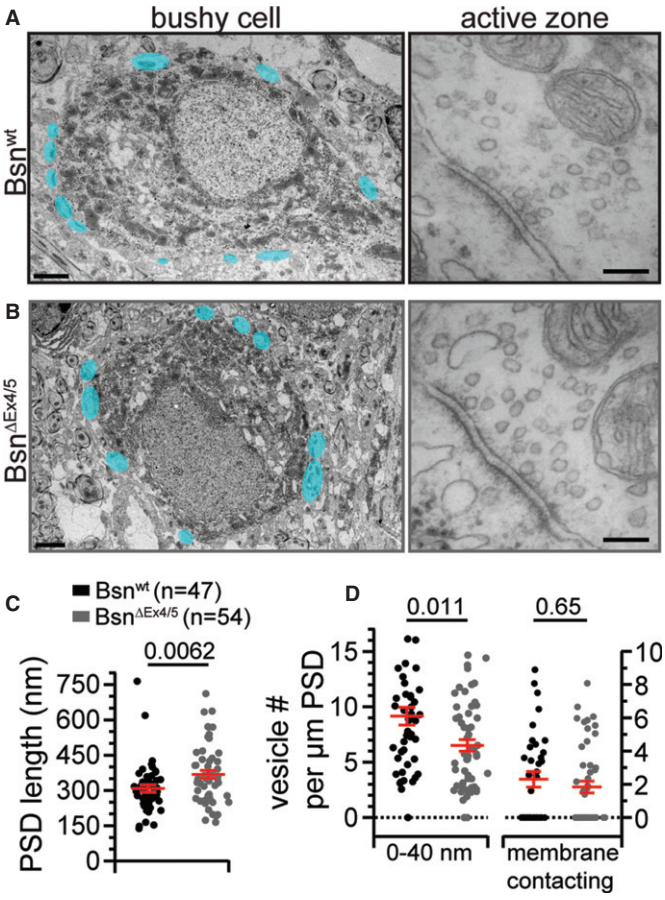

Figure 3. Ultrastructural analysis reveals an increase in PSD length in $Bsn^{\Delta Ex4/5}$ endbulbs.

A, B Example electron micrographs of Bsn^{wt} (A) and $Bsn^{\Delta Ex4/5}$ (B) bushy cells (scale bars, 2 µm) and endbulb of Held synapse AZs (scale bars, 100 nm). Structures highlighted in cyan represent asymmetric, excitatory presynaptic terminals onto the postsynaptic soma.

C The length of the postsynaptic density (PSD) was significantly increased in $Bsn^{\Delta Ex4/5}$ endbulb synapses.

D When normalized to PSD length, vesicle counts in the first bin were significantly decreased, but the number of vesicles in direct contact with the presynaptic plasma membrane remained unchanged.

the reduced membrane capacitance in $Bsn^{\Delta Ex4/5}$ BCs (11.6 ± 0.33 pF in $Bsn^{\Delta Ex4/5}$, $n = 47$ vs. 14.32 ± 0.49 pF in Bsn^{wt} $n = 56$, $P = 1 \times 10^{-5}$; data set of Table 1). There was a small but insignificant trend towards larger input resistance in $Bsn^{\Delta Ex4/5}$ BCs. Resting membrane potential and membrane time constant of BCs were not significantly different between both genotypes.

Increased release probability, decreased RRP size and slower vesicle replenishment

In order to unravel potential effects of bassoon disruption on evoked transmission we applied a minimal stimulation protocol to study the BC response to input of an individual ANF. We placed a monopolar electrode in the vicinity of the recorded BC in acute sagittal AVCN slices (Yang & Xu-Friedman, 2008) and distinguished BCs from

Table 1. Largely preserved basal synaptic transmission at BSN$^{\Delta Ex4/5}$ synapses

Initial EPSC ($EPSC_1$)	Bsn^{wt} $n = 56$	$Bsn^{\Delta Ex4/5}$ $n = 47$	*P*-value
Amplitude (nA)	10.9 ± 0.85 (0.58)[#]	10.1 ± 0.91 (0.62)	0.49
10–90% rise time (ms)	0.20 ± 0.01 (0.36)	0.23 ± 0.01 (0.31)	0.012
FWHM (ms)	0.48 ± 0.01 (0.22)	0.54 ± 0.02 (0.21)	0.01
τ_{decay} (ms)	0.17 ± 7 × 10^{-6} (0.29)	0.21 ± 8 × 10^{-6} (0.3)	0.0001
Synaptic latency (ms)	0.66 ± 0.03 (0.29)	0.75 ± 0.04 (0.33)	0.14
AMPA/NMDA*	8.32 ± 1.6 (0.72)	7.93 ± 1.2 (0.47)	0.81

*AMPA/NMDA ratio was measured in a subset of cells: $n = 15$ and $n = 10$, respectively.
[#]The *P*-values are provided and significance is indicated by $P < 0.05$.

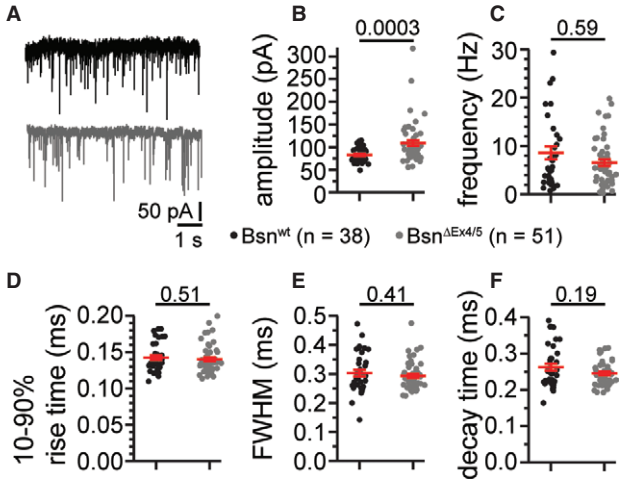

Figure 4. Increase in quantal size at BSN$^{\Delta Ex4/5}$ synapses.

A Representative traces of spontaneous mEPSCs (Bsn^{wt} in black, $Bsn^{\Delta Ex4/5}$ in grey).

B The amplitude of mEPSCs was significantly increased in $Bsn^{\Delta Ex4/5}$ BCs.

C–F The frequency (C) and kinetics - rise time (D), full-width at half-maximum (FWHM; E) and decay time (F) were not significantly altered.

stellate cells by the characteristic kinetics of their postsynaptic currents and their short-term plasticity (Chanda & Xu-Friedman, 2010b). This functional distinction was confirmed by inspection of cell morphology after filling them with the fluorescent dye Alexa-488 via the pipette in a subset of experiments (Supplementary Fig S4). The mean amplitude of the EPSC elicited by a single stimulation was unchanged despite the larger quantal size in $Bsn^{\Delta Ex4/5}$ endbulbs, while the kinetics was slightly slower (Fig 5A, Table 1). The unchanged AMPA/NMDA ratio indicated normal synaptic maturation in $Bsn^{\Delta Ex4/5}$ endbulbs (Table 1).

Next, we studied short-term plasticity by applying 20 consecutive stimuli at 100, 200 or 333 Hz, which represent firing frequencies naturally occurring in auditory nerve fibers (Taberner & Liberman, 2005). Responses of $Bsn^{\Delta Ex4/5}$ endbulbs showed faster and stronger depression with lower steady-state values (Fig 5A,B,D,E; Table 2). Stronger depression was also evident from the lower paired-pulse ratio for the responses to the first two pulses at all stimulus frequencies (Table 2). The lower paired-pulse ratio and faster decline of responses during the train indicated an increased release probability in the $Bsn^{\Delta Ex4/5}$ endbulb synapses (see below). We estimated release probability, size of the readily releasable pool of vesicles (RRP) and vesicle replenishment by applying the method of integration (Schneggenburger *et al*, 1999) to the EPSC trains (Fig 5F). Line fitting to the last 10 of the 20 data points was used to estimate the number of readily releasable vesicles (the ordinate crossing of the extrapolated line-fit divided by the mean mEPSC amplitude) and to approximate vesicle replenishment (slope of fit), which are summarized in Table 2. In brief, we found a decreased RRP size for all stimulus frequencies and an increased release probability for 333 Hz stimulation. We then focused our analysis on responses to 100 Hz stimulation, since there, the short-term depression phenotype of $Bsn^{\Delta Ex4/5}$ was most pronounced. Receptor desensitization seemed not to contribute substantially to the stronger depression in $Bsn^{\Delta Ex4/5}$ synapses as the competitive AMPA receptor antagonist kynurenic acid (1 mM) did not alter the normalized BC responses (Fig 5C; $Bsn^{\Delta Ex4/5}$: $n = 38$, $Bsn^{\Delta Ex4/5}$+kyn: $n = 8$). Next, we probed whether the synaptic phenotype may arise from a dominant negative effect from the $Bsn^{\Delta Ex4/5}$ fragment by analyzing the responses of BCs to 100 Hz ANF stimulation in heterozygous mice (Bsn^{het}). We did not find a significant difference compared to Bsn^{wt} responses (Supplementary Fig S5) and, moreover, observed punctate bassoon (Bsn-sap7f) immunofluorescence colocalizing with piccolo immunofluorescent spots, indicative of proper targeting of the full-length bassoon expressed from one allele to active zones (Supplementary Fig S5).

Seeking to further study the hypothesis of a reduced replenishment rate, we probed the recovery from depression by measuring the EPSC amplitude at varying time points after a conditioning train of 20 stimuli at 100 Hz (Fig 6; Bsn^{wt}: $n = 11$–16, $Bsn^{\Delta Ex4/5}$: $n = 5$–13). The time course of recovery was best described by a double exponential function. Time constants for the fast component were 47.9 and 90.4 ms, and for the slow component 2.81 and 3.64 s for Bsn^{wt} and $Bsn^{\Delta Ex4/5}$, respectively (fits constrained to reach 100%). A linear fit to the first four data points (25–100 ms) after the end of the conditioning train, serving as a measure for the initial rate of recovery, revealed a shallower slope for $Bsn^{\Delta Ex4/5}$ (364.1 vs. 492.9%/s for Bsn^{wt}) synapses, indicating a slowed initial rate of recovery in the absence of functional bassoon.

During and after the train we observed more asynchronous release in $Bsn^{\Delta Ex4/5}$ synapses, which we attribute to the increased release probability (Fig 7A,B; Bsn^{wt}: $n = 25$, $Bsn^{\Delta Ex4/5}$: $n = 28$; data of Fig 5). The number of asynchronous EPSCs was significantly increased also after 200 and 333 Hz stimulation in $Bsn^{\Delta Ex4/5}$ synapses (Supplementary Fig S6), but again, the difference was greatest for 100 Hz trains. Using the current-clamp mode we showed that the enhanced asynchronous release triggered misplaced spikes following the train of stimulation (Fig 7; Bsn^{wt}: $n = 10$, $Bsn^{\Delta Ex4/5}$: $n = 18$). Forty percent of $Bsn^{\Delta Ex4/5}$ BCs spiked at least once after cessation of stimulation, while no misplaced spikes were found in Bsn^{wt} synapses. In summary, we found a reduction of vesicle replenishment and size of the standing RRP whereas release probability was increased. We argue that these opposing effects and the increased quantal size lead to an unaltered response to single stimuli.

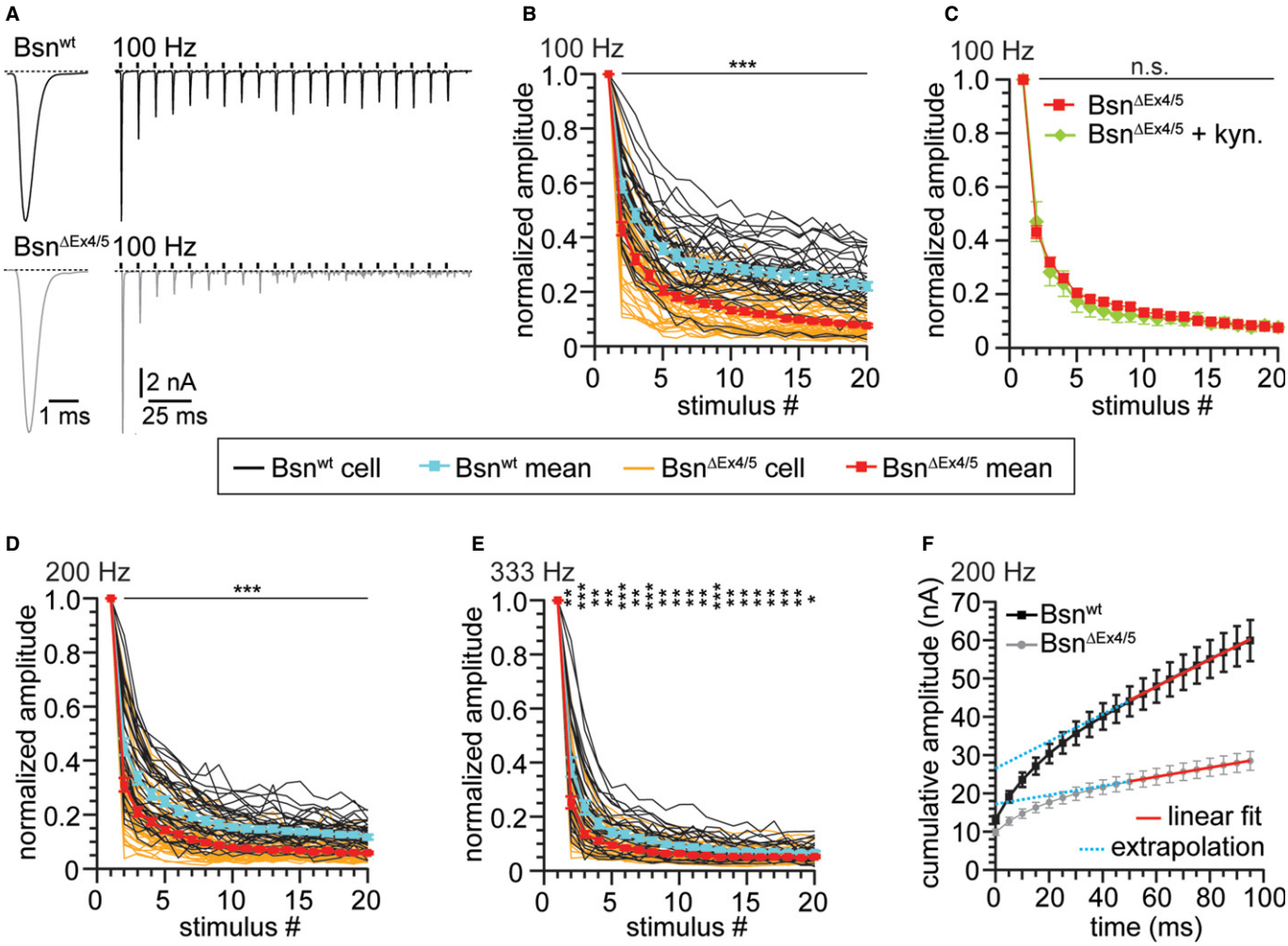

Figure 5. Stronger depression during high-frequency stimulation at BSN$^{\Delta Ex4/5}$ synapses.

A Example traces of EPSCs evoked at 100 Hz recorded from a Bsn^{wt} and a Bsn$^{\Delta Ex4/5}$ synapse illustrating the typical fast kinetics and short-term depression of BC EPSCs in the Bsn^{wt} and the deeper depression in Bsn$^{\Delta Ex4/5}$ synapses.

B, C Short-term depression in response to (B) 20 stimuli applied at 100 Hz (n(Bsn^{wt}) = 38, n(Bsn$^{\Delta Ex4/5}$) = 46) and (C) in the presence of 1 mM kynurenic acid [n(Bsn$^{\Delta Ex4/5}$ + kyn.) = 8].

D, E Stimulation applied at (D) 200 Hz [n(Bsn^{wt}) = 36, n(Bsn$^{\Delta Ex4/5}$) = 49] and (E) 333 Hz [n(Bsn^{wt}) = 30, n(Bsn$^{\Delta Ex4/5}$) = 41]. Black traces and grey traces are mean responses from individual Bsn^{wt} and Bsn$^{\Delta Ex4/5}$ BCs, respectively. Grand means ± SEM for control synapses are depicted in cyan for Bsn^{wt} and in red for Bsn$^{\Delta Ex4/5}$ synapses.

F For estimation of the readily releasable pool size, EPSCs from trains were plotted cumulatively and a linear fit to the last ten amplitudes was extrapolated.

Data information: *P < 0.05; **P < 0.01; ***P < 0.001.

Reliability of synaptic transmission is maintained

In order to test whether the stronger synaptic depression during train stimulation leads to more failures in the transmission of action potentials in Bsn$^{\Delta Ex4/5}$ endbulb synapses we analyzed the reliability of transmission in current clamp mode (Fig 7). As expected, Bsn^{wt} endbulbs of Held transmitted very reliably at 100 Hz. Surprisingly, mutant synapses were almost as reliable, even at the end of the stimulus train (Fig 7F). Spike latencies (Fig 7G, measured at peak) and their standard deviation (Fig 7H, spike jitter) were almost identical between both genotypes.

Next, we asked whether a homeostatic increase in BC excitability contributed to maintaining reliable synaptic transmission in the AVCN of Bsn$^{\Delta Ex4/5}$ mice. The slope conductance was comparable between BCs of both phenotypes over the range of currents injected with a small but insignificant trend towards smaller conductance in Bsn$^{\Delta Ex4/5}$ BCs (Fig 8A,B). However, Bsn$^{\Delta Ex4/5}$ BCs fired more spikes for the same current injection, which became significant for current injections of 350 pA and larger (Fig 8C; Bsn^{wt}: n = 31, Bsn$^{\Delta Ex4/5}$: n = 30). Comparing the action potentials we found a trend towards more hyperpolarized onset potentials and larger maximal potential changes (Supplementary Fig S7). Given the reduced ANF activity in Bsn$^{\Delta Ex4/5}$ mice and previous reports on deprivation-triggered homeostatic changes of the axon initial segment and its Na^+ channel complement in the avian equivalent of the AVCN (Nucleus magnocellularis; Kuba *et al*, 2010) we studied the length of the axon

Table 2. Quantification of short-term depression, pool size, release probability and vesicle replenishment

Frequency	Parameter	Bsn^{wt}	$Bsn^{\Delta Ex4/5}$	*P*-value
	q	82 pA	109 pA	
100 Hz	τ (ms)	20.16 ± 2.02	15.81 ± 1.4	0.076
	$EPSC_{18–20}/EPSC_1$	0.23 ± 0.015	0.08 ± 0.006	1.3×10^{-12}
	$EPSC_2/EPSC_1$	0.59 ± 0.023	0.43 ± 0.024	1.3×10^{-5}
	P_{vr}	0.49 ± 0.02	0.48 ± 0.02	0.63
	RRP (# vesicles)	303.39 ± 32.25	230.55 ± 22.9	0.067
	Repl. (# vesicles/ms)	3.59 ± 0.44	0.92 ± 0.10	2.0×10^{-11}
200 Hz	τ (ms)	7.45 ± 0.83	4.88 ± 0.51	0.005
	$EPSC_{18–20}/EPSC_1$	0.13 ± 0.008	0.06 ± 0.02	1.0×10^{-10}
	$EPSC_2/EPSC_1$	0.45 ± 0.031	0.31 ± 0.024	4.0×10^{-4}
	P_{vr}	0.55 ± 0.03	0.61 ± 0.02	0.12
	RRP (# vesicles)	321.29 ± 29.10	157.70 ± 14.5	1.03×10^{-6}
	Repl. (# vesicles/ms)	4.31 ± 0.47	1.1 ± 0.10	5.6×10^{-13}
333 Hz	τ (ms)	3.36 ± 0.39	2.05 ± 0.17	0.005
	$EPSC_{18–20}/EPSC_1$	0.07 ± 0.005	0.05 ± 0.004	0.015
	$EPSC_2/EPSC_1$	0.38 ± 0.036	0.25 ± 0.022	3.6×10^{-3}
	P_{vr}	0.59 ± 0.02	0.70 ± 0.02	0.007
	RRP (# vesicles)	245.34 ± 23.37	151.22 ± 16.2	7.0×10^{-4}
	Repl. (# vesicles/ms)	3.01 ± 0.32	1.61 ± 0.17	6.6×10^{-4}

q: the quantal size was taken from the mEPSC amplitude; τ: time constant of a single exponential fit to the EPSC amplitudes during train stimulation; $EPSC_{18–20}$: average amplitude of EPSCs number 18–20; P_{vr}: vesicular release probability; RRP: readily releasable pool; Repl.: replenishment of vesicles.
Estimates of the readily releasable pool (RRP), release probability and vesicle replenishment were obtained with the method of integration (Schneggenburger *et al*, 1999). A line was fitted to last 10 of 20 data points from cumulative amplitude plots and extrapolated to the ordinate crossing.

initial segment of AVCN principal neurons and recorded Na^+ currents from BCs. We used ankyrin-G immunolabeling to mark axon initial segments (Grubb & Burrone, 2010) in coronal sections of the brainstem and measured their apparent length in projections of confocal sections of the AVCN (Fig 8E). While this analysis underestimated their true length, differences in length should nonetheless be revealed. We did not observe significant differences in apparent length, neither along the dorsoventral tonotopic gradient (Wickesberg & Oertel, 1988) in either genotype, nor did we find systematic differences between both genotypes (Fig 8F). Next we recorded Na^+/action currents from BC by somatic patch-clamp. In order to improve voltage-clamp we reduced the Na^+ current amplitude by partial tetrodotoxin (20 nM) block. We did not find significant differences between BCs of both genotypes (Fig 8G, H; Bsn^{wt}: $n = 10$, $Bsn^{\Delta Ex4/5}$: $n = 11$). Together, an unchanged apparent length of axon initial segments and unchanged Na^+/action current amplitudes suggest that BCs do not upregulate their axosomatic Na^+ channel complement to counteract the reduced afferent input.

Partial restoration of synchronous auditory signaling in the AVCN

Synchronous activity in the auditory nerve is diminished in $Bsn^{\Delta Ex4/5}$ as a result of disrupting the afferent synapse of inner hair cells (Khimich *et al*, 2005). The compound action potential of the auditory nerve (wave 1 of the auditory brainstem response) is reduced to an extent exceeding the decrease of single ANF firing, which is likely explained by an increased temporal jitter of the first spike of ANF (Buran *et al*, 2010). However, the wave 2 of auditory brainstem response, reflecting synchronous activity of the AVCN, is much less affected (e.g. Supplementary Fig S8) and this has been attributed to an improved rate and/or timing of BC firing due to converging input from several ANF (Khimich *et al*, 2005; Buran *et al*, 2010; Jing *et al*, 2013). However, neither this hypothesis nor the impact of bassoon disruption on transmission at the endbulb synapse have been addressed by *in vivo* recordings of sound driven activity from single BCs. We studied the activity of putative BCs of the AVCN of 3- to 8-week-old $Bsn^{\Delta Ex4/5}$ and Bsn^{wt} mice (Fig 9). We differentiated ANFs and putative BCs based on the position of the microelectrode and the peristimulus time histogram (see Materials and Methods). We also included previously analyzed ANF (Jing *et al*, 2013) for the comparison to BCs. As reported earlier, we found a reduction of evoked spike rates in $Bsn^{\Delta Ex4/5}$ ANFs (Buran *et al*, 2010; Frank *et al*, 2010). However, the spike rate at sound onset of putative mutant BCs was slightly less reduced than in ANFs, indicating that brainstem mechanisms partially counteract the cochlear deficit to recover spike rates (Fig 9C; $Bsn^{\Delta Ex4/5}$ ANF: $n = 32$, $Bsn^{\Delta Ex4/5}$ AVCN: $n = 12$). The $Bsn^{\Delta Ex4/5}$ adapted rate, on the other hand, was affected to a similar extent as in ANFs (Fig 9D). In order to elucidate how bassoon disruption at the endbulb synapses affects transmission of auditory information in the AVCN, we compared BC firing in $Bsn^{\Delta Ex4/5}$ and Bsn^{wt} mice while matching ANF activity between both genotypes. We reduced the sound pressure levels for Bsn^{wt} mice so that their ANF adapted spike rates matched the maximal adapted firing rate of $Bsn^{\Delta Ex4/5}$

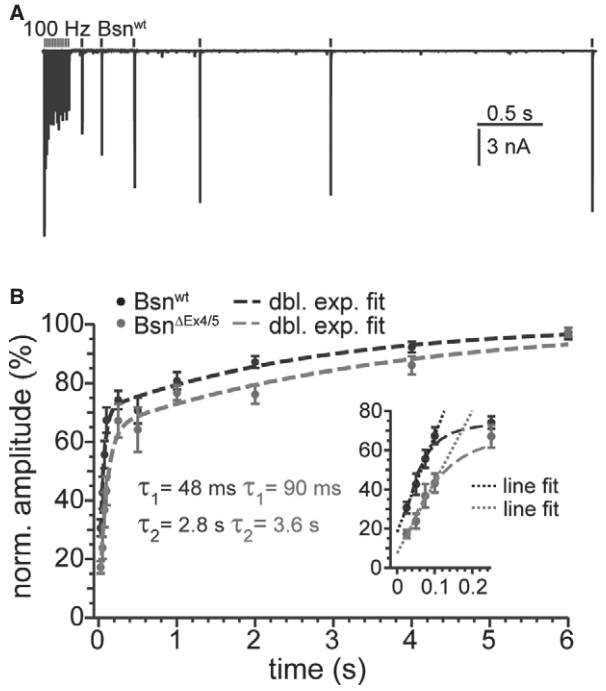

Figure 6. Recovery from short-term depression is slowed in $Bsn^{\Delta Ex4/5}$ synapses.

After a conditioning train of 20 stimuli at 100 Hz, recovery from depression was probed by single stimuli evoked after (in ms) 25, 50, 75, 100, 250, 500 (further in s) 1, 2, 4 and 6.

A Overlay of six recordings of a Bsn^{wt} bushy cell, in which recovery was tested at different times between 100 ms and 4 s.

B Plots mean (±SEM) percentage of the recovery of EPSC amplitude with respect to the first EPSC amplitude of the train. Dashed lines are double exponential fits. The inset shows the first five responses in detail. Dotted lines represent linear regressions to the first four responses approximating the initial rate of recovery.

ANF (Supplementary Fig S8). We found comparable rates in BCs of $Bsn^{\Delta Ex4/5}$ and Bsn^{wt} mice (Supplementary Fig S8) suggesting no further impairment in afferent auditory transmission at endbulb synapses due to bassoon disruption. In summary, these *in vivo* findings corroborate our hypothesis that due to homeostatic plasticity afferent auditory transmission from ANFs to BCs is intact at least at the firing rates of $Bsn^{\Delta Ex4/5}$ ANF amenable to sound stimulation. We propose that homeostatic plasticity and convergence of inputs likely underlie the improved sound onset firing of BCs and the better preserved wave 2 of the auditory brainstem response.

Discussion

We demonstrated a role of the presynaptic scaffold protein bassoon in synaptic transmission at the endbulb of Held synapse. We provide evidence that bassoon promotes a large readily releasable pool and efficient vesicular replenishment at these high-throughput synapses. However, bassoon-deficiency did not significantly alter the reliability of synaptic transmission at the rates of stimulation studied. Instead, the firing rates of BCs at sound onset were slightly higher than those of ANF. We propose that homeostatic plasticity by pre- and postsynaptic upscaling of endbulb synapses and increased intrinsic excitability of BCs together with convergence of ANFs onto BCs improve synchronous signalling in the dysfunctional auditory pathway of $Bsn^{\Delta Ex4/5}$ mutants.

Molecular composition of endbulb AZs and effects of bassoon-disruption

Apart from its peripheral origin (Farago *et al*, 2006; Kelley, 2006), the endbulb differs from other CNS presynaptic terminals by its large size, the large number of AZs and its capacity for fast and temporally precise transmission. Here we provide first insights into the molecular composition of the AZs in endbulbs of Held showing the presence of the CAZ proteins bassoon, piccolo, Munc13-1, RIM2, CAST and ELKS. For bassoon and its homologue piccolo, a role in the formation and maintenance of AZs has been proposed soon after their discovery (Friedman *et al*, 2000; Zhai *et al*, 2000). However, partial deletion or knock-down of either bassoon or piccolo had little effect on the morphology of conventional AZs (Altrock *et al*, 2003; Mukherjee *et al*, 2010). In line with these previous observations, we found a normal number of endbulbs and AZs per BC as well as a largely intact ultrastructure of endbulb AZs in $Bsn^{\Delta Ex4/5}$ mutants. The unaltered AMPA/NMDA ratio indicates maturity of the endbulb synapses (Isaacson & Walmsley, 1995; Futai *et al*, 2001) arguing against developmental deficits, as they were observed in hippocampal mossy fiber terminals of bassoon mutants (Lanore *et al*, 2010). Loss of functional bassoon from the CAZ network did neither reduce the number of excitatory synapses nor prevent integration of piccolo, Munc13-1 and RIM2 into the CAZ. The observed upregulation of piccolo at $Bsn^{\Delta Ex4/5}$ AZs together with the overlap in protein interactions (Wang *et al*, 2009) leads us to suggest that piccolo compensates for the loss of some of bassoon's function(s) at central synapses. This is in line with a recent demonstration that knock-down of all piccolo and bassoon isoforms was required to disrupt the integrity of presynaptic terminals of hippocampal cultured neurons, ultimately leading to degradation of the synapse (Waites *et al*, 2013).

Synaptic transmission in bassoon-deficient synapses

Transmission in $Bsn^{\Delta Ex4/5}$ endbulbs of Held showed several differences compared to Bsn^{wt} controls. Our main findings are a larger quantal size, an increased release probability, a decreased RRP size and slowed vesicular replenishment. We suggest that the increase in quantal size reflects an increased abundance of AMPA receptors within the enlarged PSD, because neither VGLUT1 immunofluorescence nor EM measurements of vesicle size indicated a presynaptic origin. Since the increase in quantal size was not found in previous studies on other bassoon-deficient synapses (Altrock *et al*, 2003; Hallermann *et al*, 2010) we favor the interpretation that it reflects synaptic scaling of the endbulbs in response to partial sensory deprivation (see below). An increase in release probability was indicated by faster and stronger depression and enhanced asynchronous release. The paired-pulse ratio was smaller for $Bsn^{\Delta Ex4/5}$ endbulbs at all stimulus rates, while the speed of depression and the estimate of release probability from the EPSC-integration technique differed significantly only at 200 and 333 Hz, respectively. The enhancement of

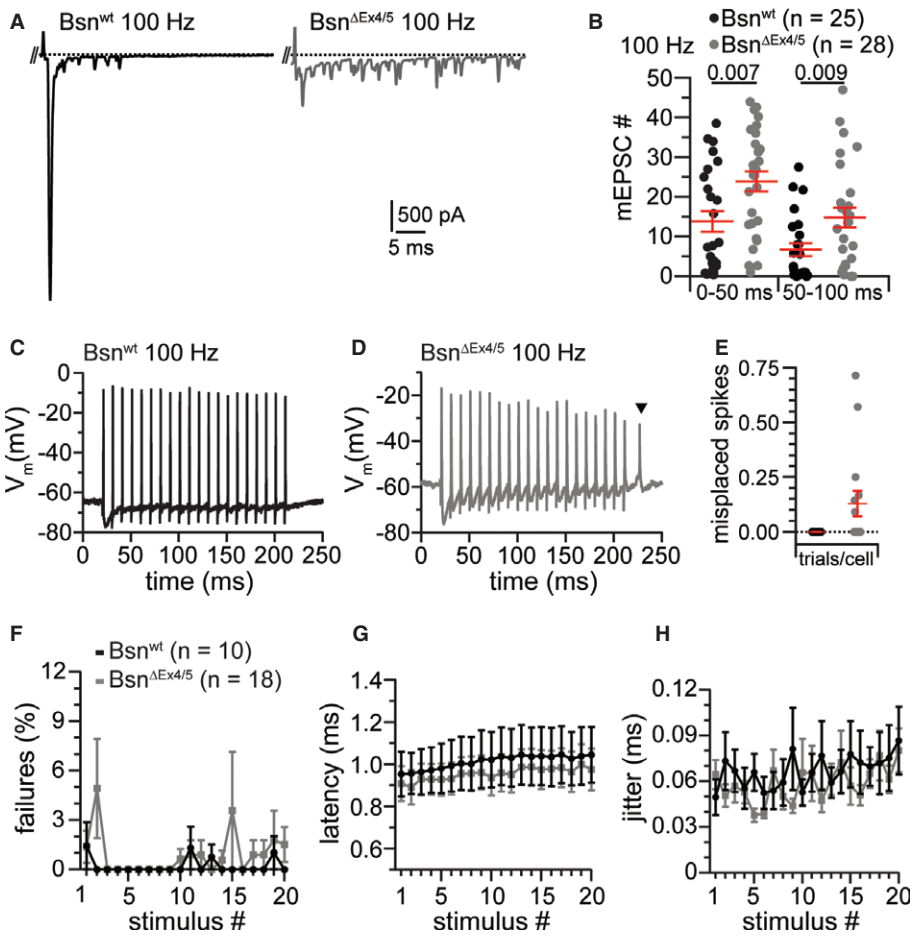

Figure 7. Increased asynchronous release leads to misplaced spikes in Bsn$^{\Delta Ex4/5}$ BCs.

A Example traces of asynchronous release events after a 100 Hz train. The positive peak at the beginning of the displayed trace is the last stimulus artifact followed by the last evoked release event of the train response. The following peaks represent spontaneous EPSCs.

B Significantly more delayed EPSCs occur in Bsn$^{\Delta Ex4/5}$ synapses as shown for two 50 ms bins after train stimulation at 100 Hz.

C, D Example traces of a Bsn^{wt} (C) and a Bsn$^{\Delta Ex4/5}$ (D) BCs action potential train following 20 stimuli at a frequency of 100 Hz. Note the occurrence of a misplaced spike in the mutant after stimulation has ceased (triangle).

E While misplaced spikes did not occur in Bsn^{wt} BCs, misplaced spikes were detected in approximately 12% of all Bsn$^{\Delta Ex4/5}$ trials per cell (40% of the Bsn$^{\Delta Ex4/5}$ BCs fired at least one misplaced spike).

F Both, Bsn^{wt} and Bsn$^{\Delta Ex4/5}$ BCs followed 100 Hz minimal stimulation reliably.

G, H The spike latency, measured from the start of the stimulus to the peak of the action potential, and its jitter (expressed as the standard deviation of the latency) were not significantly altered in Bsn$^{\Delta Ex4/5}$ synapses.

release probability might have been revealed by the EPSC-integration technique only with most rapid RRP depletion protocol (at 333 Hz), because at lower stimulation rates the method tends to overestimate the RRP, and consequently, to underestimate release probability in Bsn$^{\Delta Ex4/5}$ synapses due to their lower rate of vesicle replenishment. Impaired replenishment might also explain why the mEPSC frequency rate was unchanged despite the increased release probability.

It is not trivial to decipher whether the increased release probability resulted from a direct effect of bassoon disruption or from a possible homeostatic adaptation to the reduced afferent input (Oleskevich & Walmsley, 2002; Oleskevich *et al*, 2004; Cao *et al*, 2008) resulting from the hair cell synapse defect (Khimich *et al*, 2005; Buran *et al*, 2010; Jing *et al*, 2013). We addressed the underlying molecular mechanism by estimating the abundance of the candidate regulators of release probability RIM, Munc13-1 and VGLUT1 (Betz *et al*, 2001; Han *et al*, 2011; Weston *et al*, 2011; Fernández-Busnadiego *et al*, 2013) and did not encounter obvious changes in their immunofluorescence at the Bsn$^{\Delta Ex4/5}$ endbulbs. However, we found a reduced abundance of the novel candidate effector protein of bassoon, Mover. Mover is a small vesicle associated protein that has been identified based on its interaction with bassoon (Kremer *et al*, 2007) and has been proposed to negatively regulate release probability (Körber, 2011). It is tempting to speculate that Mover is downregulated in the absence of bassoon and that this contributes to the observed increase in release probability in bassoon-deficient endbulb synapses. The downregulation of Mover unlikely reflects a general synaptic

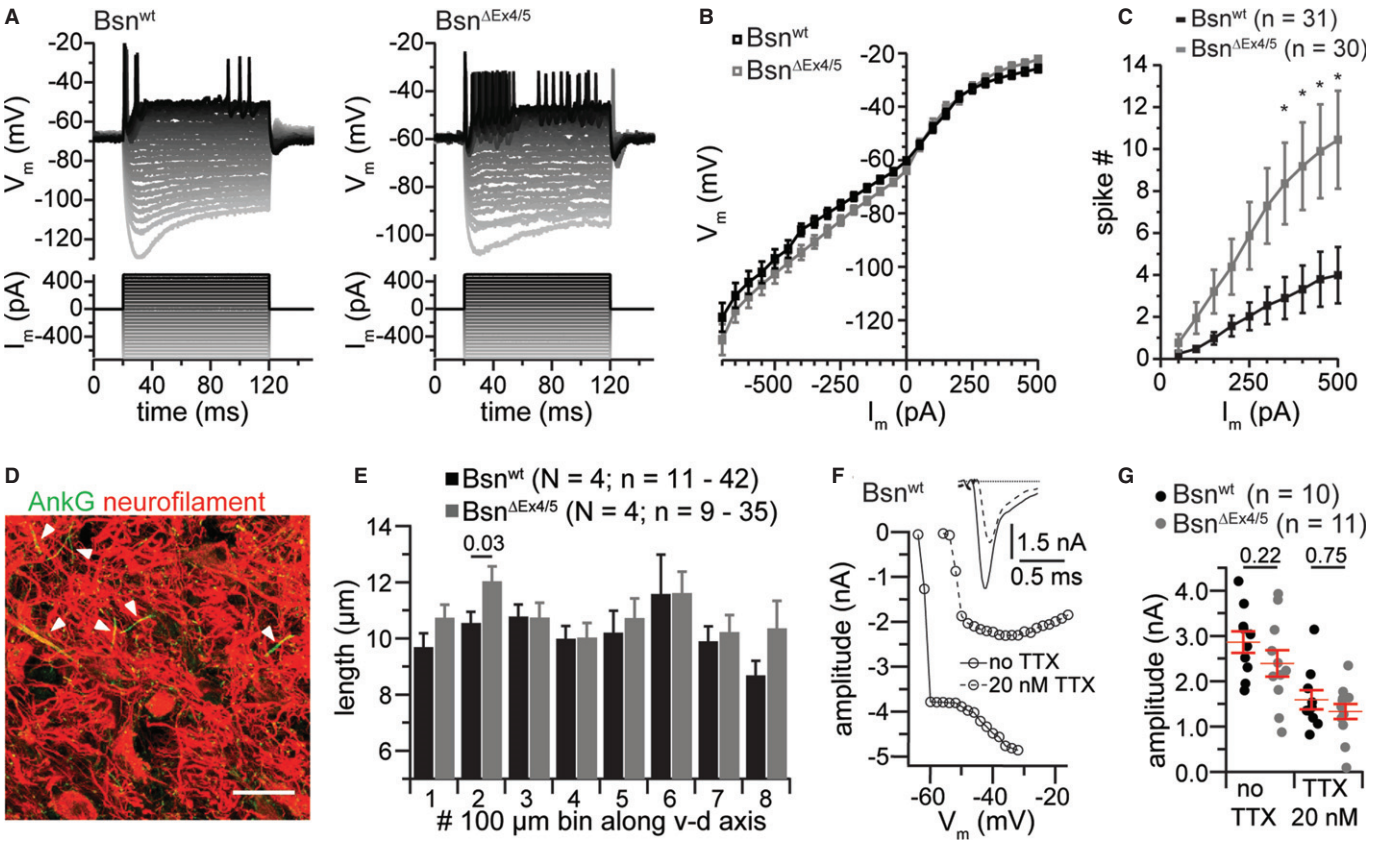

Figure 8. Bsn$^{\Delta Ex4/5}$ BCs fire more spikes in response to depolarizing current injection.

A, B Example traces of V_m (top) of a Bsn^{wt} and a Bsn$^{\Delta Ex4}$/5 BC in response to the step current injections (bottom) used for comparing the VI-relationship in the beginning of a depolarizing current step (B).

C The number of spikes during depolarizing current steps was larger in mutant compared to Bsn^{wt} BCs.

D Example confocal image of axon initial segments (AIS) in the AVCN obtained from ankyrin-G (AnkG) immunolabeling costained for neurofilament.

E The apparent AIS length averaged in eight 100 nm bins from the ventral to dorsal axis of the AVCN was largely unchanged in mutant principal cells.

F After identification of bushy cells by their phasic firing, K^+ currents were blocked and I–V relationships were recorded. Transient inward currents probably represented unclamped action currents and partial block by bath application of 20 nM TTX reduced the amplitude by ~55% but did not enable clamping the voltage at the AIS as indicated by the all-or-none-like current and the relatively constant peak current amplitudes, exemplified in (G). The inset shows an example current at -40 mV before (solid line) and after application of 20 nM TTX (dashed line).

G No significant difference was observed between current amplitudes of Bsn$^{\Delta Ex4/5}$ and Bsn^{wt} BCs, before and after application of TTX when stepping to −40 mV.

degeneration since the abundance of other presynaptic proteins was maintained (Munc13, RIM, VGLUT1) or even enhanced (piccolo). It remains possible that increase of release probability reflects a presynaptic homeostatic adaptation in response to the partial auditory deprivation, which would be consistent with our finding of normal Mover levels in Bsn$^{\Delta Ex4/5}$ inhibitory terminals. It will be interesting in future experiments to address the role of Mover at the endbulb synapse by genetic disruption, to test the presynaptic homeostatic plasticity hypothesis by studying spiral ganglion neuron (SGN) specific bassoon disruption, and, if positive, to explore the relevance of mechanisms that were previously reported to regulate presynaptic homeostatic plasticity (Kim & Ryan, 2010; Lazarevic *et al*, 2011; Müller & Davis, 2012) at the endbulb synapse.

The integration technique revealed a significant reduction of the RRP size for all stimulation frequencies. The morphological correlate of the physiologically defined RRP is subject to active research. It may not only include 'membrane contacting' or 'docked' vesicles, which were not changed in number at AZs of Bsn$^{\Delta Ex4/5}$ endbulbs, but potentially also membrane proximal tethered vesicles (Siksou *et al*, 2009). We found a significant reduction of membrane proximal vesicles per µm PSD, which seems consistent with the functional finding of a reduced RRP. However, EM tomography required to resolve tethers, was not employed. In addition, there may be fewer functional release sites due to fewer presynaptic Ca^{2+} channels. A reduction in the number of AZ Ca^{2+} channels was indeed reported for bassoon-deficient synapses of photoreceptors and hair cells (tom Dieck *et al*, 2005; Frank *et al*, 2010), though this may be partly explained by a role of the synaptic ribbon to promote clustering of Ca^{2+} channels (Frank *et al*, 2010; Jing *et al*, 2013). Finally, the standing RRP, resulting from the balance of release and replenishment (Frank *et al*, 2010; Pangršič *et al*, 2010; Oesch & Diamond, 2011), may be lower due to impaired vesicle replenishment. Indeed, we found evidence for impaired replenishment during

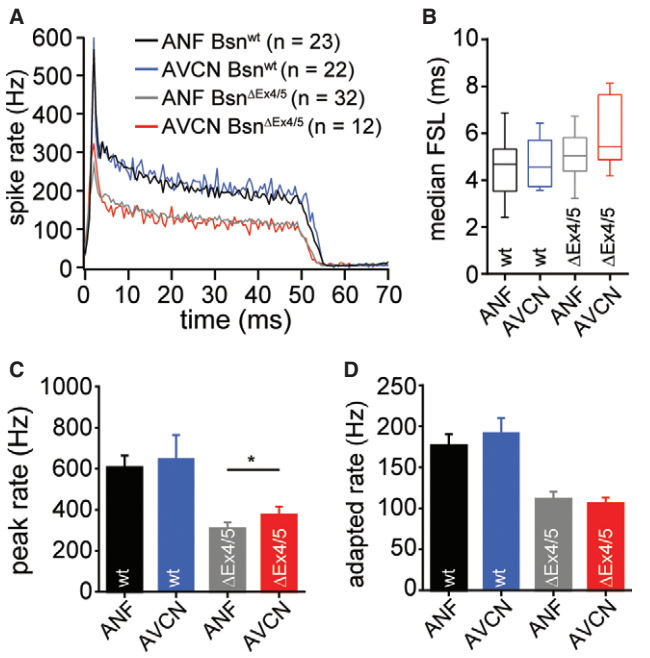

Figure 9. Partial recovery of spiking at sound-onset in Bsn$^{\Delta Ex4/5}$ BCs.

A Average PSTH of putative AVCN and ANF units of Bsn$^{\Delta Ex4/5}$ and Bsn^{wt} mice. PSTHs were aligned to the bin of their respective median first spike latency before averaging.

B Increased median first spike latency (FSL) in AVCN and ANF of Bsn$^{\Delta Ex4/5}$ mice. Note that FSL does not allow separation of AVCN and ANF.

C, D Quantification of peak (1 ms bin from the median FSL) and adapted spike rates (last 5 ms response of 50 ms tone burst) showing that the AVCN Bsn$^{\Delta Ex4/5}$ peak rate was significantly larger than the peak rate of Bsn$^{\Delta Ex4/5}$ ANF.

and after stimulation. Probing the recovery from depression, we observed a slowing of the fast component of recovery similar to what was previously found at the cerebellar mossy fibers to granule cell synapse, another high-throughput connection (Hallermann *et al*, 2010). Bassoon might contribute to efficient re-supply of vesicles (Hallermann & Silver, 2013) which is compatible with its tens of nanometer extension into the cytosol (Dani *et al*, 2010; Limbach *et al*, 2011). While bassoon seems not to directly bind to synaptic vesicles, Mover might act as an adapter.

Convergent input and homeostatic plasticity in the AVCN improve auditory signaling in bassoon mutant mice

The impaired sound coding at bassoon-deficient hair cell synapses (Khimich *et al*, 2005; Buran *et al*, 2010; Frank *et al*, 2010; Jing *et al*, 2013) leads to reduced afferent input into the cochlear nucleus. Given drastic reduction of the spiral ganglion compound action potential, the better preserved amplitudes of the second peak of auditory brainstem responses that reflects AVCN activity (Melcher *et al*, 1996) had remained puzzling. Here, we demonstrate that in Bsn$^{\Delta Ex4/5}$ mice the onset firing of BCs was slightly improved over that of ANFs. We postulate that homeostatic plasticity (Turrigiano, 2011) in the AVCN, likely induced by the partial auditory deprivation due to the synaptic defect in hair cells, together with the convergence of ANF in the AVCN (Cao & Oertel, 2010) account for the partially restored sound onset response. Our study suggests that both synaptic and intrinsic homeostatic mechanisms increase the excitability of BCs. Postsynaptic upscaling and the decreased soma size of BCs jointly reduce the presynaptic input required for supra-threshold depolarization. Our interpretation is in agreement with previous morphological analyses of endbulbs in congenitally deaf and chemically deafened cats reporting increased PSD length and decreased BC size (Pasic & Rubel, 1989; Baker *et al*, 2010; Ryugo *et al*, 2010). Interestingly, incompletely deafened cats with residual hearing showed intermediate phenotypes and the phenotype of deaf cats could be ameliorated by electrical stimulation of auditory nerve fibers with cochlear implants (Ryugo *et al*, 2005; O'Neil *et al*, 2011). Future experiments will be required to study the regulation, e.g. a potential role of Arc/Arg3.1 (Bramham *et al*, 2008), and the precise molecular changes accompanying the homeostatic plasticity observed at the endbulb synapse in the AVCN in response to auditory deprivation.

Materials and Methods

Animals

Mice with deletion of exons 4 and 5 of the Bassoon gene (Altrock *et al*, 2003) (Bsn$^{\Delta Ex4/5}$) and their wild-type littermates (Bsn^{wt}) were studied from postnatal day 15 to 23. They were derived from heterozygous breeding with C57BL/6J genetic background (following backcrossing over seven generations). PCR was used for genotyping.

In vitro electrophysiology

Parasagittal slices (150 μm) of cochlear nuclei were prepared as described (Yang & Xu-Friedman, 2008). Briefly, brains were carefully dissected and immediately immersed in ice-cold low-sodium, low-calcium slicing solution containing (in mM): NaCl (75), $NaHCO_3$ (26), sucrose (75), NaH_2PO_4 (1.25), KCl (2.5), glucose (25), $MgCl_2$ (7) and $CaCl_2$ (0.25), aerated with carbogen (95% O_2—5% CO_2); osmolarity of the solution was ~312 mOsm. After the meninges were removed from the ventral aspect of the brainstem the two hemispheres were separated by a hemisection through the median plane and the forebrain was removed at the pons-midbrain junction. Both sides of the brainstem were glued onto the stage of a Leica (Wetzlar, Germany) 1200 S vibrating microtome with the lateral aspect of the brainstem facing upwards, allowing for parasagittal sectioning. Slices were allowed to recover for 30 min in artificial cerebrospinal fluid (aCSF) heated to 34°C before being used for electrophysiological experiments. aCSF contained (in mM): NaCl (125), $NaHCO_3$ (26), glucose (15), KCl (2.5), NaH_2PO_4 (1.25), $MgCl_2$ (1), $CaCl_2$ (1.5), Na L-lactate (4), Na pyruvate (2), Na L-ascorbate (0.4), and was aerated with carbogen at all times. The Mg^{2+} and Ca^{2+} concentrations were chosen to match closely as possible the *in vivo* CSF concentrations (Jones & Keep, 1988; Sun *et al*, 2009). Experiments were carried out under constant superfusion with pre-warmed aCSF at flow rates of 3–4 ml/min. The temperature was monitored by a thermistor placed between inflow site and tissue

slice and warmed to 34–36°C by an inline solution heater (SH-27B with TC-324B controller; Warner Instruments, Hamden, CT, USA).

Pipettes were pulled with a filament puller (P-97; Sutter Instrument, Novato, CA, USA) from borosilicate glass (outer diameter: 1.5 mm, inner diameter: 0.86 mm; Science Products, Hofheim, Germany) and had resistances of 1.5–3 MΩ when filled with internal solution for voltage clamp containing (in mM): CsF (35), CsCl (100), EGTA (10), HEPES (10), and QX-314 (1; Alomone Labs, Jerusalem, Israel); or alternatively for current clamp (in mM): 130 $KMeSO_3$ (130), NaCl (10), HEPES (10), $MgCl_2$ (2), EGTA (0.5), $CaCl_2$ (0.16), MgATP (4), NaGTP (0.4), Na_2Phosphocreatine (14), with pH adjusted to 7.3, and an osmolarity of 300 mOsm. Mean series resistance was around 5 MΩ and routinely compensated by 70%. Presynaptic auditory nerve fibers were stimulated using a monopolar electrode in a glass capillary (patch pipette) filled with aCSF. The stimulation electrode was placed at a minimum distance of one cell diameter away from the cell being recorded and currents of 3–20 μA were delivered through a stimulus isolator (A360 World Precision Instruments, Sarasota, FL, USA). Miniature excitatory post-synaptic currents (mEPSCs) were initially recorded in the presence of 0.5 mM TTX (Tocris, Ellisville, USA), but as reported (Isaacson & Walmsley, 1996; Lu *et al*, 2007) no difference in the mEPSCs were noted if recorded without TTX and hence, most of the recordings were carried out without TTX with the benefit of being able to confirm the cell type by evoking synaptic transmission after recording of mEPSCs. To prevent AMPA receptor saturation/desensitization 1 mM kynurenic acid (Tocris) was added to the aCSF in some experiments. Unless otherwise noted, chemicals were purchased from Sigma-Aldrich (St. Louis, USA).

Single-unit recordings from auditory nerve and anteroventral cochlear nucleus

In vivo experiments were performed as described (Taberner & Liberman, 2005; Jing *et al*, 2013). After induction of anesthesia with urethane (1.32 mg/kg), xylazine (5 mg/kg) and buprenorphine (0.1 mg/kg), the animals were tracheostomized and the cartilaginous ear canals were removed before they were positioned in a custom-designed headholder and stereotactic apparatus. An occipital approach with partial removal of occipital bone and cerebellum was applied to expose the surface of the cochlear nucleus. For auditory nerve recordings, a glass microelectrode was advanced through the posterior end of the anteroventral cochlear nucleus, targeting nerve fibers with a primary-like response pattern near the internal auditory canal. For AVCN recordings, a more anterior position was preferred to avoid the auditory nerve and instead target the area where a higher fraction of spherical BCs is located. After the spontaneous rate, characteristic frequency (CF) and best threshold for each unit were measured, 200 repetitions of 50 ms tone bursts at CF, 30 dB above threshold (2.5 ms $\cos^2$ rise/fall, repetition rate 8 Hz) were used to characterize sound-evoked responses. Sound-responsive units were classified as BCs when their response pattern was 'pri-notch' or when it was 'primary-like' and the stereotactic position was at a depth of < 1 mm below the surface of the cochlear nucleus and/or anterior of the internal auditory canal. Extracellular signals were amplified and bandpass filtered (300–3000 Hz) using an ELC-03XS amplifier (NPI Electronic, Tamm, Germany). Digitized signals (Tucker Davis Technologies System 3, Alachua, FL, USA) were saved for offline analysis using custom-written Matlab software (Mathworks, Natick, MA, USA).

Immunohistochemistry and confocal imaging

Brains were dissected as for electrophysiology and frozen in 2-methylbutane at −35 to −40°C. After equilibration to cutting temperature (chamber: −22°C, object stage: −20°C, Figocut E cryotome; Reichert-Jung, Depew, NY, USA) 30 μm thick coronal cryosections were cut and collected onto gelatin-coated object slides. For comparison of both genotypes via parallel processing, we collected one slice of each genotype per object slide. For fixation, object slides were immersed in ice-cold formaldehyde diluted to 4% with phosphate buffered saline (PBS) for 2 min. Thereafter, the slices were washed for 30 min in PBS and incubated for 1 h in Goat Serum Dilution Buffer (GSDB: 16% normal goat serum, 450 mM NaCl, 0.3% Triton X-100, 20 mM phosphate buffer, pH 7.4) in a wet chamber at room temperature. Primary antibodies (Supplementary materials) were dissolved in GSDB buffer and applied overnight at 4°C in a wet chamber. After washing 2 × 5 min with wash buffer (wash buffer: 450 mM NaCl, 20 mM phosphate buffer, 0.3% Triton X-100) and 2 × 5 min in PBS the tissue was incubated with secondary antibodies (Supplementary materials) in GSDB in a wet light-protected chamber for 1 h at room temperature. Then, the slices were washed 2 × 5 min in wash buffer, 2 × 5 min in PBS and 1 × 5 min in 5 mM phosphate buffer, and finally mounted with a drop of fluorescence mounting medium based on Mowiol 4–88 (Carl Roth, Karlsruhe, Germany) and DABCO (Carl Roth) and covered with a thin glass cover slip.

Confocal images were acquired using a laser-scanning confocal microscope (Leica TCS SP5; Leica Microsystems CMS) equipped with 488 nm (Ar) and 561/633 nm (He–Ne) lasers for excitation of the respective Alexa fluorophore and a 63×/1.4 NA oil-immersion objective. Stacks of confocal images were collected with step sizes of 0.20–0.25 μm and a pixel size of 48 nm. Samples of $Bsn^{\Delta Ex4/5}$ and Bsn^{wt} mice were processed in parallel and images were taken with the same settings preferentially during the same imaging session.

Electron microscopy

Animals were transcardially perfused with 4% formaldehyde and parasagittal slices from cochlear nuclei were obtained as for physiology. Subsequently, slices were fixed 60 min on ice with secondary fixative comprising 2% glutaraldehyde in 0.1 M sodium cacodylate buffer, pH 7.2, washed in sodium cacodylate buffer and postfixed on ice for 1 h with 1% osmium tetroxide (in 0.1 M sodium cacodylate buffer), followed by a 1 h washing step in sodium cacodylate buffer and three brief washing steps in distilled water. The samples were stained en bloc with 1% uranyl acetate in distilled water for 1 h on ice. After a brief wash with distilled water, samples were dehydrated at room temperature in increasing ethanol concentrations, infiltrated in Epon resin (100% EtOH/Epon 1:1, 30 and 90 min; 100% Epon, overnight), and embedded for 48 h at 70°C. Following conventional embedding 55–60 nm sections were cut approaching from the anterior edge. Slices were postfixed and stained with uranyl acetate/lead citrate following standard protocols. Micrographs were taken with a 1024 × 1024 charge-coupled device

detector (HSS 512/1024; Proscan Electronic Systems, Scheuering, Germany) in an electron microscope (EM 902A; Carl Zeiss, Inc., Oberkochen, Germany) operated in bright field mode or with a JEOL electron microscope (JEM 1011, JEOL, Eching, Germany) equipped with a GatanOrius 1200A camera (Gatan, Munich, Germany) using the Gatan Digital Micrograph software package.

Data analysis

Data analysis was performed using Matlab (Mathworks), Igor Pro (Wavemetrics, Lake Oswego, OR, USA), Mini Analysis (Synaptosoft Inc., Fort Lee, NJ, USA) and ImageJ software (Schneider *et al*, 2012). Figures were assembled for display in the Adobe Illustrator (Adobe Systems, Munich, Germany) software. Means are presented with their standard errors (SEM) and represent grand averages of the cell's means (unless stated otherwise). Statistically significant differences between groups were determined by either using unpaired, two-tailed Student's *t*-tests (if data was distributed normally and the variances between the groups were comparable), or Wilcoxon Rank tests where data distribution did not fulfill the mentioned criteria. Normality was tested with the Jarque-Bera (Jarque & Bera, 1987) test, and variances were compared with the *F*-test. Reconstruction of endbulb terminals from calretinin-stained confocal image stacks was done by visually tracing, labeling and computed volume rendering with the Reconstruct software (Fiala, 2005). For Fig 2G, single confocal images were analyzed by averaging fluorescence intensities from regions of interest defined by suprathreshold pixels in either the VGLUT1 or the VGAT channel, representing endbulb and inhibitory terminals, respectively. For Figs 1D–G and 2A–F, stacks of confocal images were analyzed with a custom written Matlab routine described earlier (Meyer *et al*, 2009) with modifications for ameliorating the intensity differences within a stack by linearly increasing the threshold. This allowed for localizing the center of mass (center of immunofluorescence mass coordinates were calculated by the average pixel position weighted by pixel intensity) from weakly fluorescent spots as well as separation of closely spaced fluorescent spots with high fluorescence intensities.

Supplementary information for this article is available online: http://emboj.embopress.org

Acknowledgments

We thank S. Gerke and C. Senger-Freitag for expert technical assistance and G. Hoch for developing image analysis routines. We thank Eckart Gundelfinger for providing $Bsn^{\Delta Ex4/5}$ mice. We thank Matthew Xu-Friedman for training in BC recordings to A.M.S. and for comments on the manuscript. This work was supported by the German Research Foundation through the Göttingen Graduate School for Neurosciences, Biophysics and Molecular Biosciences (GSC 226/1, excellence fellowship to A.M.S.), Center for Nanoscopy and Molecular Physiology of the Brain (to T.M.) and Collaborative Sensory Research Center 889 to T.M. (project A5), N.S. (project A6), C.W. (project A7) and T.D. (project B2) and the German Federal Ministry of Education and Research (through the Bernstein Center grant 01GQ0433 to T.M.

Author contributions

This study was conceived by T.M. and A.M.S. The experimental work was performed by A.M.S. (BC patch clamp, immunohistochemistry, contribution to electron microscopy), Z.J. (*in vivo* single unit recordings), F.W. (immunohistochemistry) and C.W. (electron microscopy). J.M.S.C. contributed to image analysis. A.M.S., T.M., C.W., N.S. and T.D. prepared the manuscript.

Conflict of interest

The authors declare that they have no conflict of interest.

References

Alabi AA, Tsien RW (2012) Synaptic vesicle pools and dynamics. *Cold Spring Harb Perspect Biol* 4: a013680

Altrock WD, tom Dieck S, Sokolov M, Meyer AC, Sigler A, Brakebusch C, Fässler R, Richter K, Boeckers TM, Potschka H, Brandt C, Löscher W, Grimberg D, Dresbach T, Hempelmann A, Hassan H, Balschun D, Frey JU, Brandstätter JH, Garner CC (2003) Functional inactivation of a fraction of excitatory synapses in mice deficient for the active zone protein bassoon. *Neuron* 37: 787 – 800

Babalian AL, Jacomme A-V, Doucet JR, Ryugo DK, Rouiller EM (2002) Commissural glycinergic inhibition of bushy and stellate cells in the anteroventral cochlear nucleus. *NeuroReport* 13: 555 – 558

Baker CA, Montey KL, Pongstaporn T, Ryugo DK (2010) Postnatal development of the endbulb of held in congenitally deaf cats. *Front Neuroanat* 4: 19

Betz A, Thakur P, Junge HJ, Ashery U, Rhee J-S, Scheuss V, Rosenmund C, Rettig J, Brose N (2001) Functional interaction of the active zone proteins Munc13-1 and RIM1 in synaptic vesicle priming. *Neuron* 30: 183 – 196

Bramham CR, Worley PF, Moore MJ, Guzowski JF (2008) The immediate early gene arc/arg3.1: regulation, mechanisms, and function. *J Neurosci* 28: 11760 – 11767

Buran BN, Strenzke N, Neef A, Gundelfinger ED, Moser T, Liberman MC (2010) Onset coding is degraded in auditory nerve fibers from mutant mice lacking synaptic ribbons. *J Neurosci* 30: 7587 – 7597

Caicedo A, d' Aldin C, Eybalin M, Puel JL (1997) Temporary sensory deprivation changes calcium-binding proteins levels in the auditory brainstem. *J Comp Neurol* 378: 1 – 15

Cao XJ, McGinley MJ, Oertel D (2008) Connections and synaptic function in the posteroventral cochlear nucleus of deaf jerker mice. *J Comp Neurol* 510: 297 – 308

Cao X-J, Oertel D (2010) Auditory nerve fibers excite targets through synapses that vary in convergence, strength, and short-term plasticity. *J Neurophysiol* 104: 2308 – 2320

Carlson SS, Valdez G, Sanes JR (2010) Presynaptic calcium channels and α3-integrins are complexed with synaptic cleft laminins, cytoskeletal elements and active zone components. *J Neurochem* 115: 654 – 666

Chanda S, Xu-Friedman MA (2010a) Neuromodulation by GABA converts a relay into a coincidence detector. *J Neurophysiol* 104: 2063 – 2074

Chanda S, Xu-Friedman MA (2010b) A low-affinity antagonist reveals saturation and desensitization in mature synapses in the auditory brain stem. *J Neurophysiol* 103: 1915 – 1926

Chen J, Billings SE, Nishimune H (2011) Calcium channels link the muscle-derived synapse organizer laminin B2 to bassoon and CAST/Erc2 to organize presynaptic active zones. *J Neurosci* 31: 512 – 525

Dani A, Huang B, Bergan J, Dulac C, Zhuang X (2010) Superresolution imaging of chemical synapses in the brain. *Neuron* 68: 843 – 856

Dick O, Hack I, Altrock WD, Garner CC, Gundelfinger ED, Brandstätter JH (2001) Localization of the presynaptic cytomatrix protein Piccolo at

ribbon and conventional synapses in the rat retina: comparison with Bassoon. *J Comp Neurol* 439: 224 – 234

Dick O, tom Dieck S, Altrock WD, Ammermüller J, Weiler R, Garner CC, Gundelfinger ED, Brandstätter JH (2003) The presynaptic active zone protein bassoon is essential for photoreceptor ribbon synapse formation in the retina. *Neuron* 37: 775 – 786

tom Dieck S, Altrock WD, Kessels MM, Qualmann B, Regus H, Brauner D, Fejtová A, Bracko O, Gundelfinger ED, Brandstätter JH (2005) Molecular dissection of the photoreceptor ribbon synapse: physical interaction of Bassoon and RIBEYE is essential for the assembly of the ribbon complex. *J Cell Biol* 168: 825 – 836

tom Dieck S, Sanmartí-Vila L, Langnaese K, Richter K, Kindler S, Soyke A, Wex H, Smalla KH, Kämpf U, Fränzer JT, Stumm M, Garner CC, Gundelfinger ED (1998) Bassoon, a novel zinc-finger CAG/glutamine-repeat protein selectively localized at the active zone of presynaptic nerve terminals. *J Cell Biol* 142: 499 – 509

Dondzillo A, Sätzler K, Horstmann H, Altrock WD, Gundelfinger ED, Kuner T (2010) Targeted three-dimensional immunohistochemistry reveals localization of presynaptic proteins Bassoon and Piccolo in the rat calyx of Held before and after the onset of hearing. *J Comp Neurol* 518: 1008 – 1029

Dresbach T, Hempelmann A, Spilker C, tom Dieck S, Altrock WD, Zuschratter W, Garner CC, Gundelfinger ED (2003) Functional regions of the presynaptic cytomatrix protein bassoon: significance for synaptic targeting and cytomatrix anchoring. *Mol Cell Neurosci* 23: 279 – 291

Farago AF, Awatramani RB, Dymecki SM (2006) Assembly of the brainstem cochlear nuclear complex is revealed by intersectional and subtractive genetic fate maps. *Neuron* 50: 205 – 218

Fernández-Busnadiego R, Asano S, Oprisoreanu A-M, Sakata E, Doengi M, Kochovski Z, Zürner M, Stein V, Schoch S, Baumeister W *et al* (2013) Cryo-electron tomography reveals a critical role of RIM1α in synaptic vesicle tethering. *J Cell Biol* 201: 725 – 740

Fiala JC (2005) Reconstruct: a free editor for serial section microscopy. *J Microsc* 218: 52 – 61

Frank T, Rutherford MA, Strenzke N, Neef A, Pangršič T, Khimich D, Fejtova A, Gundelfinger ED, Liberman MC, Harke B, Bryan KE, Lee A, Egner A, Riedel D, Moser T (2010) Bassoon and the synaptic ribbon organize Ca^2+ channels and vesicles to add release sites and promote refilling. *Neuron* 68: 724 – 738

Friedman HV, Bresler T, Garner CC, Ziv NE (2000) Assembly of new individual excitatory synapses: time course and temporal order of synaptic molecule recruitment. *Neuron* 27: 57 – 69

Futai K, Okada M, Matsuyama K, Takahashi T (2001) High-fidelity transmission acquired via a developmental decrease in NMDA receptor expression at an auditory synapse. *J Neurosci* 21: 3342 – 3349

Gómez-Nieto R, Rubio ME (2009) A bushy cell network in the rat ventral cochlear nucleus. *J Comp Neurol* 516: 241 – 263

Grubb MS, Burrone J (2010) Activity-dependent relocation of the axon initial segment fine-tunes neuronal excitability. *Nature* 465: 1070 – 1074

Gundelfinger ED, Fejtova A (2012) Molecular organization and plasticity of the cytomatrix at the active zone. *Curr Opin Neurobiol* 22: 423 – 430

Hallermann S, Fejtova A, Schmidt H, Weyhersmüller A, Silver RA, Gundelfinger ED, Eilers J (2010) Bassoon speeds vesicle reloading at a central excitatory synapse. *Neuron* 68: 710 – 723

Hallermann S, Silver RA (2013) Sustaining rapid vesicular release at active zones: potential roles for vesicle tethering. *Trends Neurosci* 36: 185 – 194

Han Y, Kaeser PS, Südhof TC, Schneggenburger R (2011) RIM determines Ca^{2+} channel density and vesicle docking at the presynaptic active zone. *Neuron* 69: 304 – 316

Haucke V, Neher E, Sigrist SJ (2011) Protein scaffolds in the coupling of synaptic exocytosis and endocytosis. *Nat Rev Neurosci* 12: 127 – 138

Isaacson JS, Walmsley B (1995) Receptors underlying excitatory synaptic transmission in slices of the rat anteroventral cochlear nucleus. *J Neurophysiol* 73: 964 – 973

Isaacson JS, Walmsley B (1996) Amplitude and time course of spontaneous and evoked excitatory postsynaptic currents in bushy cells of the anteroventral cochlear nucleus. *J Neurophysiol* 76: 1566 – 1571

Jarque CM, Bera AK (1987) A test for normality of observations and regression residuals. *Int Stat Rev* 55: 163

Jing Z, Rutherford MA, Takago H, Frank T, Fejtova A, Khimich D, Moser T, Strenzke N (2013) Disruption of the presynaptic cytomatrix protein bassoon degrades ribbon anchorage, multiquantal release, and sound encoding at the hair cell afferent synapse. *J Neurosci* 33: 4456 – 4467

Jones HC, Keep RF (1988) Brain fluid calcium concentration and response to acute hypercalcaemia during development in the rat. *J Physiol* 402: 579 – 593

Kelley MW (2006) Regulation of cell fate in the sensory epithelia of the inner ear. *Nat Rev Neurosci* 7: 837 – 849

Khimich D, Nouvian R, Pujol R, tom Dieck S, Egner A, Gundelfinger ED, Moser T (2005) Hair cell synaptic ribbons are essential for synchronous auditory signalling. *Nature* 434: 889 – 894

Kim SH, Ryan TA (2010) CDK5 serves as a major control point in neurotransmitter release. *Neuron* 67: 797 – 809

Kopp-Scheinpflug C, Dehmel S, Dörrscheidt GJ, Rübsamen R (2002) Interaction of excitation and inhibition in anteroventral cochlear nucleus neurons that receive large endbulb synaptic endings. *J Neurosci* 22: 11004 – 11018

Körber C (2011) Functional characterization of the vertebrate-specific presynaptic protein Mover in the calyx of Held Funktionelle Charakterisierung des vertebratenspezifischen präsynaptischen Proteins Mover im Heldschen Calyx. Ruperto-Carola University of Heidelberg.

Kremer T, Kempf C, Wittenmayer N, Nawrotzki R, Kuner T, Kirsch J, Dresbach T (2007) Mover is a novel vertebrate-specific presynaptic protein with differential distribution at subsets of CNS synapses. *FEBS Lett* 581: 4727 – 4733

Kuba H, Oichi Y, Ohmori H (2010) Presynaptic activity regulates Na+ channel distribution at the axon initial segment. *Nature* 465: 1075 – 1078

Lanore F, Blanchet C, Fejtova A, Pinheiro P, Richter K, Balschun D, Gundelfinger E, Mulle C (2010) Impaired development of hippocampal mossy fibre synapses in mouse mutants for the presynaptic scaffold protein Bassoon. *J Physiol* 588: 2133 – 2145

Lazarevic V, Schöne C, Heine M, Gundelfinger ED, Fejtova A (2011) Extensive remodeling of the presynaptic cytomatrix upon homeostatic adaptation to network activity silencing. *J Neurosci* 31: 10189 – 10200

Limbach C, Laue MM, Wang X, Hu B, Thiede N, Hultqvist G, Kilimann MW (2011) Molecular in situ topology of Aczonin/Piccolo and associated proteins at the mammalian neurotransmitter release site. *Proc Natl Acad Sci* 108: E392 – E401

Lohmann C, Friauf E (1996) Distribution of the calcium-binding proteins parvalbumin and calretinin in the auditory brainstem of adult and developing rats. *J Comp Neurol* 367: 90 – 109

Lu Y, Harris JA, Rubel EW (2007) Development of spontaneous miniature EPSCs in mouse AVCN neurons during a critical period of afferent-dependent neuron survival. *J Neurophysiol* 97: 635 – 646

Melcher JR, Guinan JH Jr, Knudson IM, Kiang NYS (1996) Generators of the brainstem auditory evoked potential in cat II. Correlating lesion sites with waveform changes. *Hear Res* 93: 28 – 51

Meyer AC, Frank T, Khimich D, Hoch G, Riedel D, Chapochnikov NM, Yarin YM, Harke B, Hell SW, Egner A *et al* (2009) Tuning of synapse number, structure and function in the cochlea. *Nat Neurosci* 12: 444 – 453

Mukherjee K, Yang X, Gerber SH, Kwon HB, Ho A, Castillo PE, Liu X, Südhof TC (2010) Piccolo and bassoon maintain synaptic vesicle clustering without directly participating in vesicle exocytosis. *Proc Natl Acad Sci* 107: 6504

Müller M, Davis GW (2012) Transsynaptic control of presynaptic Ca^{2+} influx achieves homeostatic potentiation of neurotransmitter release. *Curr Biol* 22: 1102 – 1108

Neher E, Sakaba T (2008) Multiple roles of calcium ions in the regulation of neurotransmitter release. *Neuron* 59: 861 – 872

Nicol MJ, Walmsley B (2002) Ultrastructural basis of synaptic transmission between endbulbs of held and bushy cells in the rat cochlear nucleus. *J Physiol* 539: 713

Oesch NW, Diamond JS (2011) Ribbon synapses compute temporal contrast and encode luminance in retinal rod bipolar cells. *Nat Neurosci* 14: 1555 – 1561

Ohtsuka T, Takao-Rikitsu E, Inoue E, Inoue M, Takeuchi M, Matsubara K, Deguchi-Tawarada M, Satoh K, Morimoto K, Nakanishi H, Takai Y (2002) Cast: a novel protein of the cytomatrix at the active zone of synapses that forms a ternary complex with RIM1 and munc13-1. *J Cell Biol* 158: 577 – 590

Oleskevich S, Walmsley B (2002) Synaptic transmission in the auditory brainstem of normal and congenitally deaf mice. *J Physiol* 540: 447 – 455

Oleskevich S, Youssoufian M, Walmsley B (2004) Presynaptic plasticity at two giant auditory synapses in normal and deaf mice. *J Physiol* 560: 709 – 719

O'Neil JN, Connelly CJ, Limb CJ, Ryugo DK (2011) Synaptic morphology and the influence of auditory experience. *Hear Res* 279: 118 – 130

Pangršič T, Lasarow L, Reuter K, Takago H, Schwander M, Riedel D, Frank T, Tarantino LM, Bailey JS, Strenzke N, Brose N, Müller U, Reisinger E, Moser T (2010) Hearing requires otoferlin-dependent efficient replenishment of synaptic vesicles in hair cells. *Nat Neurosci* 13: 869 – 876

Pasic TR, Rubel EW (1989) Rapid changes in cochlear nucleus cell size following blockade of auditory nerve electrical activity in gerbils. *J Comp Neurol* 283: 474 – 480

Rutherford MA, Pangršič T (2012) Molecular anatomy and physiology of exocytosis in sensory hair cells. *Cell Calcium* 52: 327 – 337

Ryugo D, Kretzmer E, Niparko J (2005) Restoration of auditory nerve synapses in cats by cochlear implants. *Science* 310: 1490

Ryugo DK, Baker CA, Montey KL, Chang LY, Coco A, Fallon JB, Shepherd RK (2010) Synaptic plasticity after chemical deafening and electrical stimulation of the auditory nerve in cats. *J Comp Neurol* 518: 1046 – 1063

Schneggenburger R, Meyer AC, Neher E (1999) Released fraction and total size of a pool of immediately available transmitter quanta at a calyx synapse. *Neuron* 23: 399 – 409

Schneider CA, Rasband WS, Eliceiri KW (2012) NIH Image to ImageJ: 25 years of image analysis. *Nat Meth* 9: 671 – 675

Siksou L, Varoqueaux F, Pascual O, Triller A, Brose N, Marty S (2009) A common molecular basis for membrane docking and functional priming of synaptic vesicles. *Eur J Neurosci* 30: 49 – 56

Südhof TC (2012) The presynaptic active zone. *Neuron* 75: 11 – 25

Sun L, Kosugi Y, Kawakami E, Piao Y-S, Hashimoto T, Oyanagi K (2009) Magnesium concentration in the cerebrospinal fluid of mice and its response to changes in serum magnesium concentration. *Magnes Res* 22: 266 – 272

Taberner AM, Liberman MC (2005) Response properties of single auditory nerve fibers in the mouse. *J Neurophysiol* 93: 557 – 569

Takao-Rikitsu E, Mochida S, Inoue E, Deguchi-Tawarada M, Inoue M, Ohtsuka T, Takai Y (2004) Physical and functional interaction of the active zone proteins, CAST, RIM1, and Bassoon, in neurotransmitter release. *J Cell Biol* 164: 301 – 311

Turrigiano G (2011) Too many cooks? Intrinsic and synaptic homeostatic mechanisms in cortical circuit refinement. *Annu Rev Neurosci* 34: 89 – 103

Von Gersdorff H, Borst JGG (2002) Short-term plasticity at the calyx of held. *Nat Rev Neurosci* 3: 53 – 64

Waites CL, Leal-Ortiz SA, Okerlund N, Dalke H, Fejtova A, Altrock WD, Gundelfinger ED, Garner CC (2013) Bassoon and Piccolo maintain synapse integrity by regulating protein ubiquitination and degradation. *EMBO J* 32: 954 – 969

Wang X, Hu B, Zieba A, Neumann NG, Kasper-Sonnenberg M, Honsbein A, Hultqvist G, Conze T, Witt W, Limbach C, Geitmann M, Danielson H, Kolarow R, Niemann G, Lessmann V, Kilimann MV (2009) A protein interaction node at the neurotransmitter release site: domains of Aczonin/Piccolo, Bassoon, CAST, and rim converge on the N-terminal domain of Munc13-1. *J Neurosci* 29: 12584 – 12596

Wang Y, O'Donohue H, Manis P (2011) Short-term plasticity and auditory processing in the ventral cochlear nucleus of normal and hearing-impaired animals. *Hear Res* 279: 131 – 139

Weston MC, Nehring RB, Wojcik SM, Rosenmund C (2011) Interplay between VGLUT isoforms and endophilin A1 regulates neurotransmitter release and short-term plasticity. *Neuron* 69: 1147 – 1159

Wickesberg RE, Oertel D (1988) Tonotopic projection from the dorsal to the anteroventral cochlear nucleus of mice. *J Comp Neurol* 268: 389 – 399

Wu SH, Oertel D (1984) Intracellular injection with horseradish peroxidase of physiologically characterized stellate and bushy cells in slices of mouse anteroventral cochlear nucleus. *J Neurosci* 4: 1577 – 1588

Yang H, Xu-Friedman MA (2008) Relative roles of different mechanisms of depression at the mouse endbulb of Held. *J Neurophysiol* 99: 2510 – 2521

Zhai R, Olias G, Chung WJ, Lester RAJ, tom Dieck S, Langnaese K, Kreutz MR, Kindler S, Gundelfinger ED, Garner CC (2000) Temporal appearance of the presynaptic cytomatrix protein bassoon during synaptogenesis. *Mol Cell Neurosci* 15: 417 – 428

Zhai RG, Bellen HJ (2004) The architecture of the active zone in the presynaptic nerve terminal. *Physiology* 19: 262 – 270